Engineering Fracture Mechanics 134 (2015) 368–390

Contents lists available at ScienceDirect

Engineering Fracture Mechanics

journal homepage: www.elsevier.com/locate/engfracmech

An engineering methodology for constraint corrections of elastic–plastic fracture toughness – Part I: A review on probabilistic models and exploration of plastic strain effects

Claudio Ruggieri [a,*], Robert H. Dodds Jr. [b]

[a] Dept. of Naval Architecture and Ocean Engineering, University of São Paulo, São Paulo, Brazil
[b] Dept. of Civil and Environmental Engineering, University of Illinois at Urbana-Champaign, IL, USA

ARTICLE INFO

Article history:
Received 3 March 2014
Received in revised form 15 December 2014
Accepted 19 December 2014
Available online 6 January 2015

Keywords:
Cleavage fracture
Local approach
Weibull stress
Plastic strain
Probabilistic fracture mechanics

ABSTRACT

This work describes a micromechanics methodology based upon a local criterion incorporating the effects of plastic strain on cleavage fracture coupled with statistics of microcracks. A parameter analysis is conducted under well-contained plasticity, where near-tip fields with varying constraint levels are generated through a modified boundary layer formulation. These analyses are extended to assess the effects of plastic strain on fracture toughness correlations for conventional SE(B) specimens with varying a/W-ratios. Fracture toughness predictions for a pressure vessel steel tested in the DBT transition region based on the proposed methodology are considered in Part II of this article.

1. Introduction

The fundamental importance of cleavage fracture behavior in structural integrity assessments has stimulated a rapidly increasing amount of research on predictive methodologies to quantify and analyze the influence of crack-like defects on the load carrying capacity of structural components such as, for example, cracks in critical weldments of aging structures and reactor pressure vessels (RPVs). Such methodologies play a key role in repair decisions and life-extension programs for in-service structures (*e.g.*, nuclear and pressure vessel components) while, at the same time, ensuring acceptable safety levels during normal operation. For ferritic materials at temperatures in the ductile-to-brittle transition (DBT) region, unstable fracture by transgranular cleavage represents one the most serious failure modes as local crack-tip instability may trigger catastrophic structural failure at low applied stresses with little plastic deformation.

Conventional fracture mechanics methodologies for structural integrity assessments rely on the correlation of fracture conditions across different crack geometries/loading modes as measured by the linear elastic stress intensity factor, K, or the elastic–plastic parameter defined by the J-integral and its corresponding value of the Crack Tip Opening Displacement, CTOD (δ) [1,2]. The underlying concept is that the crack-tip stress and strain fields that develop over microstructuraly significant size scales (*i.e.*, the fracture process zone of a few CTODs ahead of a macroscopic crack) can be adequately described by a single parameter, such as J, and, further, that this parameter sets the intensity of local deformation leading to material failure in various cracked structures having different levels of constraint. More recent efforts advanced the

* Corresponding author. Tel.: +55 11 30915184; fax: +55 11 30915717.
E-mail address: claudio.ruggieri@usp.br (C. Ruggieri).

http://dx.doi.org/10.1016/j.engfracmech.2014.12.015
0013-7944/

Nomenclature

α	Weibull modulus (shape parameter) of toughness distribution
α_p	Weibull modulus (shape parameter) of particle distribution
ϵ	true (logarithmic) strain
$\bar{\sigma}$	true stress
β	power-law parameter of microcrack density function
δ	crack tip opening displacement
δ_c	critical value of crack tip opening displacement
l	fractured particle size
l_c	critical size of fractured particle
l_N	reference size of fractured particle
ϵ_0	yield (reference) strain
ϵ_p	effective plastic strain
Γ	contour defined in a plane normal to the crack front
γ	Weibull modulus (shape parameter) of Weibull distribution
λ	average rate of fractured particles
μ	proportionality constant (average number of flaws exceeding a critical size per unit volume)
ν	Poisson's ratio
Ω	volume of the fracture process zone
ψ	parameter defining the size of the fracture process zone
Ψ_c	fraction of fracture particles which become eligible to propagate unstably
ρ_0	initial crack tip blunting radius
σ_0	yield (reference) stress
σ_u	Weibull stress parameter
σ_w	Beremin Weibull stress
σ_1	maximum principal stress
σ_{eq}	equivalent (effective) stress
σ_{ij}	Cartesian components of stress tensor
σ_{pf}	particle fracture stress
σ_{prs}	particle reference stress
θ	polar coordinate
$\tilde{\sigma}_w$	modified Weibull stress
$\tilde{P}$	failure probability for a stressed body
ξ	Weibull' stress dependent risk of rupture
ζ	parameter of microcrack size distribution
ζ_0	parameter of microcrack size distribution
a	microcrack size, crack depth
a_c	critical microcrack size
a_{max}	upper bound for the critical microcrack size
B	specimen thickness
b	remaining crack ligament
bcc	body cubic center
E	Young's modulus
E_d	particle's elastic modulus
f_{ij}	angular variations of in-plane stress components
J	J-integral
J_0	characteristic toughness of the Weibull distribution
J_2	second invariant of the stress deviator tensor
J_c	critical J-value (fracture toughness)
J_{min}	threshold toughness of the 3-P Weibull distribution
K	linear elastic stress intensity factor
K_I	Mode I linear elastic stress intensity factor
K_{Ic}	critical value of Mode I linear elastic stress intensity factor
K_{Jc}	critical value of the J-integral converted into K
m	Weibull modulus of Weibull stress distribution
n	Ramberg–Osgood strain hardening exponent
n_j	outward normal to Γ
P_c	probability of cleavage fracture
P_f	failure probability
P_n	probability of microcrack nucleation

P_p	probability of microcrack propagation
R	domain radius of the MBL model
r	polar coordinate
R_p	radius of the near-tip plastic region
S	specimen span
S_0	material constant (characteristic stress) in Weibull's risk of rupture
S_u	material constant (threshold stress) in Weibull's risk of rupture
T	T-stress
u	Cartesian component of displacement in X direction
u_i	Cartesian components of displacement
V	volume of material
v	Cartesian component of displacement in Y direction
V_0	reference volume
W	specimen width
W_s	stress-work density
$\mathbf{B}$	strain–displacement matrix
CTOD	Crack Tip Opening Displacement
DBT	ductile-to-brittle transition
FPZ	fracture process zone
LGC	large geometry change
MBL	modified boundary layer
PCVN	precracked Charpy specimen
pdf	probability density function
RPV	reactor pressure vessel
SE(B)	single edge notch bend specimen
SSY	small scale yielding
TSM	toughness scaling model

viewpoint of the continuum fracture mechanics framework by developing two-parameter fracture methodologies to describe the full range of Mode I, elastic–plastic crack-tip fields with varying near-tip stress triaxiality [3]. These approaches make use of the J-integral (or, equivalently, the CTOD) to scale the crack-tip fields within the near-tip region over which large stresses and strains develop, while the second parameter defines a family of crack-tip fields of varying stress triaxiality [4–10]. While all these methodologies prove sufficiently applicable to provide generally conservative acceptance criterion for cracked structural components by relating the operating conditions with a critical applied load or critical crack size, they do not address the strong sensitivity of cleavage fracture to material characteristics at the microlevel nor do they provide a more effective and yet simple procedure to predict the influence of constraint on fracture behavior.

The above arguments motivated the development of micromechanics models based upon a probabilistic interpretation of the fracture process which are most often referred to as local approaches [11–13]. Attention has been primarily focused on probabilistic models incorporating weakest link statistics to describe material failure caused by transgranular cleavage for a wide range of loading conditions and crack configurations. In particular, the seminal work of the French group Beremin [11] provides the basis for establishing a relationship between the microregime of fracture and macroscopic crack driving forces (such as the J-integral) by introducing the Weibull stress (σ_w) as a probabilistic fracture parameter. A key feature of the Beremin approach is that σ_w follows a two-parameter Weibull distribution [14] defined by the Weibull modulus, m, and the scale parameter, σ_u. Further idealization postulates that the key parameter m represents a material property in this model [11–13] which thus provides the necessary framework to correlate fracture toughness for varying crack configurations under different loading (and possibly temperature) conditions.

However, the probabilistic framework from which the Weibull stress concept is derived strongly relies upon the assumption that Griffith-like microcracks form immediately upon the onset of yielding and thus the associated statistical distribution of microcrack size remains unchanged with increased loading and deformation. Experimental evidence for the coupling between microcrack size distribution and plastic deformation has been given in the early works of McMahon and Cohen [15], Kaechele and Tetelman [16], Brindley [17], Lindley et al. [18] and Gurland [19]. These studies observed the strong effects of plastic strain on cleavage microcracking in ferritic steels at varying temperatures which can lead to a marked influence on the density of Griffith-like microcracks directly connected to the material fracture behavior at the microscale. Here, the number of microcracks formed from fractured carbide particles within a small near-tip material volume increases with increased plastic strain. Since any cleavage fracture model incorporating statistics of microcracks (weakest link philosophy), such as the σ_w-based methodology, involves a local Griffith instability of the largest of most favorably oriented microcrack, it becomes clear that increased plastic strains correlate directly with increased likelihood of cleavage failure. Indeed, a number

of important applications of the Weibull stress model to predict constraint effects on fracture toughness, including those reported by Ruggieri [20,21], were only in moderate agreement with experimentally measured J_c-values for large tension loaded cracked configurations in which large plastic strains develop. Here, application of the conventional Beremin approach yielded fracture predictions with no clear trend as the predicted toughness values were either higher or lower than the corresponding experimentally measured toughness values depending on the tested material. To some extent, these difficulties can be overcome by incorporating explicitly the influence of plastic strain into the micromechanism of cleavage failure entering directly into the probabilistic description of fracture. But how the controlling microstructural features – microcrack size distribution and plastic strain level – are interconnected and their relative contributions to the macroscopic fracture behavior (and associated failure probability) remain open issues.

This work describes a micromechanics methodology based upon a local failure criterion incorporating the effects of plastic strain on cleavage fracture coupled with statistics of microcracks. One purpose of this study is to provide an in-depth review and a theoretical description consistent with what exists for probabilistic modeling of cleavage fracture. Another is to develop limiting distributions for the cleavage fracture stress of a cracked body capable of describing the potentially strong effects of plastic strain on the cleavage failure probability. The resulting probabilistic treatment provides the basis for establishing a relationship between the microregime of fracture and macroscopic crack driving forces (such as the J-integral) by introducing a modified Weibull stress ($\tilde{\sigma}_w$) as a local crack driving force. Within the fracture mechanics framework derived here, we pursue a line of investigation in which the proposed probabilistic methodology coupling macro-scale features with the micro-scale cleavage mechanism provides an engineering approach to multiscale predictions of fracture behavior in structural components with diverse range of crack-tip constraint. This procedure is thus capable of correcting measured distributions of toughness values for fracture specimens and structural components with different geometry and loading conditions based on a relatively simple application of the toughness scaling model phrased in terms of the modified Weibull stress, $\tilde{\sigma}_w$.

A parameter analysis is conducted for stationary cracks under well-contained plasticity, where the near-tip fields of varying levels of constraint are generated through a modified boundary layer (MBL) formulation with different values of applied T-stress. A central objective is to gain some understanding on the role of plastic strain on cleavage fracture by means of the probabilistic fracture parameter and how it contributes to the cleavage failure probability. These analyses are also extended to assess the general effects of plastic strain and the associated limiting distributions on fracture toughness correlations for conventional SE(B) specimens with varying crack size over specimen width ratios. The study clearly shows important features associated with the inclusion of plastic strain effects into the Weibull stress model which are not fully accounted in conventional analyses using the standard Beremin model. Overall, inclusion of plastic strain effects into the probabilistic framework to describe cleavage fracture does reduce the amount of constraint correction from shallow-to-deep notch SE(B) fracture specimens, which is generally consistent with available toughness data. Fracture toughness predictions for a pressure vessel steel tested in the ductile-to-brittle transition region based upon the proposed methodology are considered in a forthcoming publication as Part II of this article.

2. Mechanisms and probabilistic models for cleavage fracture

The characteristic feature emerging from most probabilistic models for cleavage fracture, including the Beremin approach [11], is the adoption of a convenient statistical distribution to describe the microcrack size coupled with a weakest link concept in which macroscopic fracture behavior is controlled by unstable propagation on the microscale of the most severe Griffith-like microcrack. This feature is key to understanding the relative strengths and drawbacks of the methodology in fracture mechanics applications while, at the same time, allowing proper interpretation of the cleavage fracture process in developing an improved probabilistic model for cleavage fracture. Before introducing the statistical treatment of cleavage fracture incorporating plastic strain effects, we first provide a brief review of pertinent aspects of cleavage fracture and local approach theory which have a direct bearing on the micromechanics cleavage model addressed in the present study.

2.1. Micromechanism of cleavage fracture in structural steels

This section reviews basic features of the transgranular cleavage fracture in polycrystalline metals; this failure mode most often occurs in *bcc* metals (*e.g.*, low carbon steels) at low temperatures. A substantial number of studies and experimental observations have provided detailed descriptions of the cleavage fracture process [22–24]. It is beyond the scope of the present study to survey all the work done on cleavage fracture and associated micromechanisms. However, some general and simple concepts needed to support the fracture methodology described in the following sections are briefly introduced.

Early progress in understanding the mechanisms of brittle fracture in mild steels was achieved by means of detailed metallographic observations of cleavage microcracks. A number of works, including that of Low [25], Owen et al. [26], McMahon and Cohen [15] and Smith [24], revealed the formation of Griffith-like microcracks [27] after the onset of yielding and localized plasticity primarily by the cracking of carbides along grain boundaries. Further analyses of the microstructural features, as those represented by the early work of Curry and Knott [28,29], reveal that only *eligible* particles, which are associated with large dislocation pile-ups acting as suitable stress raisers and favorable orientation, can produce Griffith-like microcracks. This process occurs over one or two grains of the polycrystalline aggregate; once a microcrack has formed in

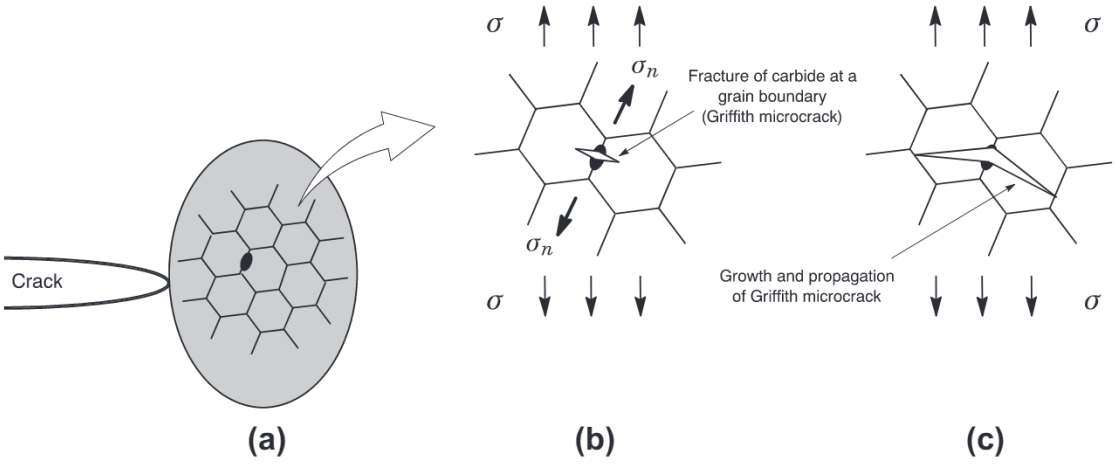

Fig. 1. Schematic of cleavage fracture due to cracking of carbides at grain boundaries of ferritic steels: (a) near-tip stressed region in connection with plastic deformation at the material microlevel; (b) fracture of carbide and formation of a Griffith-like microcrack; (c) growth of the Griffith microcrack into adjacent grains.

a grain and spread through the nearby ferrite grain boundaries, it likely propagates with no significant increase in the applied stress unless the microcrack is arrested at the grain boundary [30]. The connection between fracture resistance and microstructure can then be made by rationalizing the interrelation between microcrack nucleation and unstable propagation as illustrated in Fig. 1: (a) fracture of a carbide particle assisted by plastic deformation of the surrounding matrix nucleates a Griffith-like microcrack; (b) the nucleated microcrack advances rapidly into the interior of the ferrite grain until it reaches a grain boundary and (c) fracture occurs when the microcrack is not arrested at a grain boundary barrier and thus propagates unstably. In terms of the Griffith cleavage criterion [27], the last condition means that the Griffith fracture energy to propagate the microcrack is larger than the specific surface energy of the grain boundary [30].

More precise models to describe the cleavage fracture micromechanism should actually involve the potential void nucleation from a fractured particle in which case either the formation of a Griffith-like (sharp) microcrack is suppressed or the microcrack blunts. This process could be explicitly accounted for by formulating this concept statistically and introducing the probability that a fractured particle becomes a void directly into the probabilistic formulation. Xia and Shih [31] and Wallin and Laukkanen [32], among others, noted the competition between void nucleation and Griffith-like microcracks to arrive at a rather complex treatment associated with a conditional probability of cleavage failure. Following Hahn [30], however, we may envision a scenario whereby some microstructural features that do not influence the fraction of fractured carbides precipitating catastrophic cleavage fracture have a diminished effect, at best, on the material failure. That is, even though the number of eligible particles is relatively small compared to the actual number of carbide particles present in the steel, this small number of fractured carbides does have nonetheless a strong effect on the material cleavage fracture behavior. Only those microstructural features that effectively affect the number of eligible particles, such as plastic deformation of the surrounding matrix, can alter the material brittle behavior. Thus, neglecting the process of void nucleation from a fractured carbide still preserves the central features of the cleavage fracture mechanism entering the probabilistic formulation discussed later. Supporting evidence for this argument is given in recent work by Fairchild et al. [33] who employed scanning electron fractography to characterize the cleavage micromechanism in a microalloyed steel. Their study clearly suggests that the cleavage initiation mechanism in steels is strongly controlled by: (1) the failure strength of the particle while embedded in the ferritic matrix and (2) the interface bonding strength between the particle and the ferritic matrix. Unlike MnS, which most often tend to form voids and, therefore, have an innocuous effect on cleavage behavior, carbides and similar hard phase inclusions are likely to have a much higher interfacial strength which appears to be a key factor for cleavage microcracking.

2.2. Probabilistic approaches to cleavage fracture based on statistics of microcracks

The history of progress in probabilistic models for cleavage fracture has been one of relatively continuous development since the pioneering work of Weibull [34,35]. Early work of Epstein [36] and later Freudenthal [37] advanced the viewpoint of the weakest link concept implied in Weibull's analysis of size effects in fracture strength to introduce a mathematical description for the fracture of materials in terms of the statistical theory of extreme values [38,39]. Using purely statistical arguments, Epstein [36] showed that the distribution of the fracture strength for a stressed solid associated with the weakest link concept depends on the assumed functional form for the fracture resistance of Griffith-like microflaws randomly distributed in a given volume of material, here denoted as V. In particular, when a Gaussian distribution [14,40] is assumed to describe the probability density function (pdf) for the microflaw fracture resistance, the fracture strength of the stressed solid decreases linearly with $(\ln V)^{1/2}$, whereas when a Weibull distribution with parameters (γ, S_0) defines the pdf for the

microflaw fracture resistance then the fracture strength of the stressed solid decreases proportionally to $S_0 V^{-1/\gamma}$ [36]. Such a type of analysis, including Weibull's original work, is often referred to as the elemental strength approach [41] and derives from the premise that a stressed body contains a random distribution of Griffith-like microflaws or microcracks which can be characterized by their fracture stress at which the Griffith cleavage condition is met (termed the "microflaw strength" by Epstein [36]). Several probabilistic models have been proposed based on the elemental strength approach to develop limiting distributions for the fracture stress and to predict size effects in fracture, including the works of McClintock and Argon [42], Batdorf and Crose [43], Evans [44], McClintock and Zaverl [45], Matsuo [46], Lin et al. [47], Godse and Gurland [48], among others.

Another line of development which shares much in common with the elemental strength approach is based on the statistics of microcracks contained in the stressed material volume. A number of research efforts in this area have explicitly adopted convenient functional forms describing the microcrack size (and possibly orientation) to define a limiting distribution for the cleavage fracture stress. The early work of Freudenthal [37] devised the connection between the statistical distribution of microcrack size and the distribution function of the local fracture stress based on theoretical arguments derived from the extreme value theory [39]. Subsequent researchers adopting this class of approach include Beremin [11], Wallin et al. [49,32], Mudry [12], Pineau [50], Minami et al. [51], Ruggieri and Dodds [52], Gao et al. [53], Petti and Dodds [54] and Ruggieri [21]. Work of the French Beremin group [11] attains particular relevance as it has served as the basis for generalizing the concept of micromechanics modeling for cleavage fracture (also often referred to as local approaches) which in turn has enabled the development of approaches highly effective in unifying toughness measures across different crack configurations and loading modes. Further advancements in micromechanics modeling of cleavage fracture incorporating a more realistic physical mechanism of cleavage microcrack nucleation and propagation have also been made with the Prometey model [55–57]. An overview of these local approach developments is given by Pineau [13].

A potential drawback with the Beremin model lies in the non-recognition of the potentially strong role played by the plastic strain at the microlevel on cleavage fracture thereby ignoring the influence of the imposed near-tip stress *and* strain history on the cleavage failure probability. The Beremin approach assumes that all eligible microcracks nucleate immediately upon yielding – their distribution then does not change throughout the entire load history. Since there is a history of experimental evidence linking the increase of microcrack density with increased plastic strain [15–19], it remains apparent that further enlargement on the probabilistic framework to include plastic strain effects is needed.

More precise probabilistic models incorporating the effects of plastic strain on microcracking directed connected with the Beremin approach have been proposed by a number of authors based on the notion that the microstructural process of cleavage fracture is driven by two coupled quantities defined by the local stresses and plastic strains. Xia and Shih [31] and Bordet et al. [58,59] approached the statistical problem from the point of view of considering microcrack nucleation and propagation as two statistically independent events so that the cleavage fracture probability, P_c, is expressed by the standard product $P_n \times P_p$, where P_n is the probability of microcrack nucleation and P_p is the probability of microcrack propagation. Note here that, when $P_n = 1$ and a convenient functional form describing the microcrack size is adopted to evaluate P_p, then the cleavage fracture probability, P_c, should yield a similar expression as given by the Beremin model. Further studies of Gao et al. [60] and Ruggieri [21] focused on modifying the limiting distribution for the cleavage fracture stress by introducing a functional dependence between the microcrack density and local plastic strain directly into the probability of microcrack propagation; these workers implicitly assumed $P_n = 1$ in their models.

2.3. Fundamental statistical theory of cleavage fracture

The early work of Weibull [34,35] on the statistical description of fracture strength marks the beginning of a now rather extensive literature on statistical approaches to cleavage fracture. Two fundamental assumptions underlies Weibull's analysis: (1) the failure probability of a stressed solid with volume V is completely determined by the failure of an infinitesimally small volume dV, and (2) failure of each infinitesimally small volume dV is a statistically independent event. Making use of standard statistical procedures, the failure probability for the stressed solid, $\tilde{P}(V)$, is then defined as [37]

$$\tilde{P}(V) = 1 - e^{-\xi V} \tag{1}$$

where ξ is a constant. The above expression has a clear interpretation in which the failure probability for the stressed solid increases with increased material volume – a result entirely consistent with a purely probabilistic reasoning based on a simple application of the weakest link concept.

In fracture mechanics spirit, a more fundamental approach can be introduced by specifically considering the dependence of the fracture stress for a stressed solid on the statistical population of microflaws uniformly distributed over its volume V. Consider the stressed solid idealized as consisting of a large number of statistically independent, uniformly stressed, small volume elements, denoted δV, and assume that failure of this small volume element occurs when the size of a random flaw exceeds a critical size, *i.e.*, $a > a_c$. Two fundamental assumptions based upon probability theory and the well-known Poisson postulates (see, *e.g.*, Feller [61]) underlie the present development: (1) failures occurring in nonoverlapping volumes are statistically independent events, and (2) the probability of failure for δV is proportional to its volume, *i.e.*, $\delta\tilde{P} = \mu\delta V$ when δV is small. Here, the proportionality constant μ is the average number of flaws with size $a \geqslant a_c$ per unit volume. The elemental failure probability, $\delta\tilde{P}$, is then related to the distribution of the largest flaw in a reference volume of the material by

$$\delta\tilde{P} = \delta V \int_{a_c}^{\infty} g(a)da \tag{2}$$

where $g(a)da$ defines the probability of finding a microcracks having size between a and $a + da$ in the unit volume [41,47]. Letting $a \to \infty$ as the upper bound for the above integral is equivalent to defining a zero threshold stress for fracture; consequently, stresses vanishingly small compared to the fracture stress yield a non-zero (albeit small) probability for fracture.

While other research efforts in this area (*e.g.*, Bordet et al. [58]) advocate the use of a threshold fracture stress, in which case an upper bound for the microcrack size, a_{max}, should be introduced into Eq. (2), there is still some debate over the effectiveness of a threshold value for the fracture stress in fracture predictions. Previous study of Ruggieri and Dodds [52] has compared predictions of the variation in fracture toughness with constraint changes for a specific material using different threshold stress values and has found that adoption of zero threshold stress provides a good description for the influence of constraint on cleavage fracture toughness (J_c, δ_c). More recently, Gao and Dodds [62] have introduced a threshold parameter directly into the standard Beremin formulation which improves fracture predictions at low probabilities and, at the same time, makes contact with the statistical form adopted by ASTM E1921 [63] to describe K_{Jc}-toughness distributions for ferritic steels. Currently, we consider the correct treatment of a threshold fracture stress in the present probabilistic framework an open issue.

Now, making use of weakest link arguments in conjunction with Eq. (2) and manipulating the resulting expression, the failure probability for the stressed solid, $\tilde{P}(V)$, then becomes

$$\tilde{P}(V) = 1 - \exp\left[-\int dV \int_{a_c}^{\infty} g(a)da\right] \tag{3}$$

where it is understood that the number of statistically independent, small volume elements, $n \to \infty$ (such that $\delta V \to dV$).

A key feature of the above relation is that it allows evaluation of the fracture strength distribution for the entire volume V from the distribution of the largest flaw present in each small element δV. While a number of possible functional forms for $g(a)$ could be used, there are sound arguments (see, *e.g.*, Freudenthal [37]) that justify adoption of a distribution of extreme values [39] which also makes contact with the distribution of the largest flaw size. Here, extreme value conditions require a Cauchy-type distribution of microflaw size in the form [37,44]

$$g(a) = \frac{1}{V_0}\left(\frac{\zeta_0}{a}\right)^{\zeta} \tag{4}$$

where ζ_0 and ζ are parameters of the distribution and V_0 denotes a reference volume.

At this point, it is helpful to discuss further the nature of the microcrack size distribution given by previous Eq. (4). As already noted before in Section 2.1, only eligible carbide particles are able to fracture and thus become Griffith-like microcracks. Consequently, the distribution of microflaw size described by Eq. (4) derives from the distribution of fractured particles with size ℓ which implies that $g(a) \leftrightarrow g(\ell)$. That is, a fractured particles with size ℓ becomes a Griffith-like microcrack with size a such that both quantities are equally characterized by parameters ζ_0 and ζ defining the distribution expressed by Eq. (4). The equivalence $g(a) \leftrightarrow g(\ell)$ will also become clear in later sections addressing effects of plastic strain on cleavage fracture.

Now, the implicit distribution of fracture stress can be made explicit by introducing the dependence between the critical microcrack size, a_c, and stress in the form $a_c = K_{Ic}^2/(Y\sigma_{eq}^2)$, where K_{Ic} is the (local) fracture toughness of the material ahead of microflaw, Y represents a geometry factor and σ_{eq} denotes an *equivalent* (effective) tensile (opening) stress acting on the microcrack plane, most often adopted as the maximum principal stress, σ_1. Consequently, substituting Eq. (4) into Eq. (3) and working out the crack size integral yields the expression for $\tilde{P}(V)$ in the form

$$\tilde{P}(\sigma_1) = 1 - \exp\left[-\frac{1}{V_0}\int_V \left(\frac{\sigma_1}{\sigma_u}\right)^m dV\right] \tag{5}$$

where parameters $m = 2\zeta - 2$ and σ_u define the above fracture stress distribution.

To the extent that the fracture strength of a stressed solid containing a uniform distribution of microcracks is adequately described by the weakest link model resulting in previous Eq. (3) and, further, that extreme value conditions apply so that an inverse power-law type for the microcrack size distribution can be postulated, there is a probabilistic rationale for relating the random inhomogeneity in local features of the material with macroscopic loading through the acting stress fields as stated in the above Eq. (5). This remarkable conclusion resulting from probabilistic concepts coupled with phenomenological arguments embodies a large part of the progress achieved in micromechanics modeling of cleavage fracture over the past three decades. In particular, the Beremin model [11] derives from simply limiting the previous analysis and results to the fracture process zone (FPZ) ahead of a macroscopic crack so that Eq. (5) can be rewritten as

$$P_f(\sigma_w) = 1 - \exp\left[-\left(\frac{\sigma_w}{\sigma_u}\right)^m\right] \tag{6}$$

such that the Weibull stress, σ_w, a term coined by Beremin [11], is defined by

$$\sigma_w = \left[\frac{1}{V_0}\int_{\Omega}\sigma_1^m d\Omega\right]^{1/m} \tag{7}$$

where Ω is now the volume of the near-tip fracture process zone most often defined as the loci where $\sigma_1 \geqslant \psi\sigma_0$, with σ_0 denoting the material's yield stress and $\psi \approx 2$.

3. A Weibull stress model incorporating plastic strain effects

3.1. Probabilistic formulation

Development of a limiting distribution for the cleavage fracture stress incorporating effects of plastic strain begins by assuming the fracture process zone (FPZ) in a stressed cracked body illustrated in Fig. 2(a). The approach derives from the methodology previously outlined in Section 2.3 but with the additional condition that only microcracks formed from the cracking of brittle particles, such as carbides, in the course of plastic deformation contribute to cleavage fracture and that the fraction of fractured particles increases with increased matrix plastic strain [64]. Within the present probabilistic framework for cleavage fracture based on the statistics of microcracks, it is clearly not necessary nor essential to consider different carbide morphologies as long as the nucleated Griffith-like microcracks behave like *weakest links*. An approximate account of such a micromechanism can be made by considering that a fraction, Ψ_c, of the total number of brittle particles in the FPZ nucleates the microcracks which are eligible to propagate unstably and, further, that Ψ_c is a function of plastic strain, ϵ_p, but independent of microcrack size.

As already noted, alternative approaches to incorporate plastic strain effects into a probabilistic formulation for cleavage fracture consider a local criterion in which microcrack nucleation and propagation are treated as two statistically independent events (see, *e.g.,* Bordet et al. [58]). Here, the plastic strain enters the resulting Weibull stress formulation through the dependence of the probability of nucleating a microcrack on ϵ_p. A related approach sharing a similar philosophy has also been proposed by Margolin et al. [65,56] by addressing plastic strain effects on cleavage fracture in terms of a strain-dependent critical fracture stress. While we pursue a rather different line of investigation in the present work, it is worth noting that the adopted concept associated with *eligibility* of cleavage microcracks does not necessarily preclude the possibility of microcrack nucleation. While we recognize that the above expression describes a simple idealization of the statistical cleavage process, it is nevertheless statistically consistent while, at the same time, providing a convenient *engineering* model for fracture toughness correlations which is one of the central objectives of this work.

Now, following similar arguments to those used in Section 2.3, the elemental failure probability for the cracked body resulting from the distribution of the largest flaw present in a small volume element, δV, is given by

$$\delta P_f = \delta V \cdot \Psi_c(\epsilon_p) \cdot \int_{a_c}^{\infty} g(a)da \tag{8}$$

as pictured in Fig. 2(b). Clearly, when $\Psi_c = 1$, the above Eq. (8) yields a identical result as previous Eq. (2).

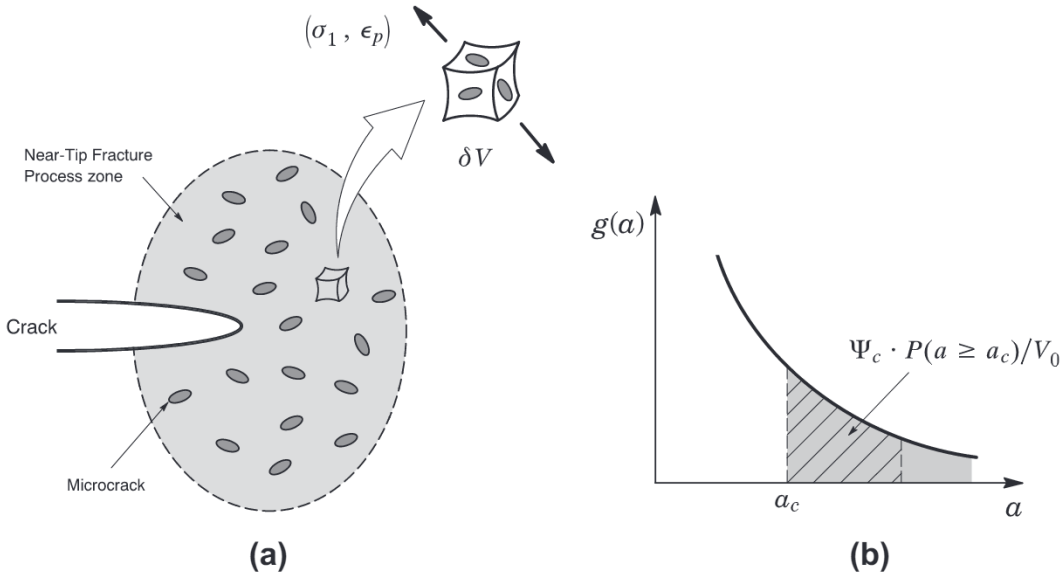

Fig. 2. (a) Near-tip fracture process zone ahead a macroscopic crack containing randomly distributed flaws. (b) Schematic of power-law type microcrack size distribution.

The same analysis as in Section 2.3 may be followed to evaluate the cleavage failure probability for the cracked body. By using the weakest link concept applied to the volume of the fracture process zone, Ω, and recalling the Cauchy-type distribution given by Eq. (4) to describe the microcrack size, one finds after little manipulation the limiting distribution for the cleavage fracture stress expressed as

$$P_f(\sigma_1, \epsilon_p) = 1 - \exp\left[-\frac{1}{V_0}\int_\Omega \Psi_c(\epsilon_p)\cdot\left(\frac{\sigma_1}{\sigma_u}\right)^m d\Omega\right] \tag{9}$$

in which the integral evaluated over Ω contains two contributions: one is from the principal stress criterion for cleavage fracture characterized in terms of σ_1 and the other is due the effective plastic strain, ϵ_p, which defines the number of eligible Griffith-like microcracks nucleated from the brittle particles effectively controlling cleavage fracture.

Again, the form of the above result motivates the notion of a modified Weibull stress, $\tilde{\sigma}_w$, defined by

$$\tilde{\sigma}_w = \left[\frac{1}{V_0}\int_\Omega \Psi_c(\epsilon_p)\cdot\sigma_1^m d\Omega\right]^{1/m} \tag{10}$$

where the volume of the fracture process zone, Ω, was previously defined in Section 2.3. Observe the coupling effect of the near-tip principal stress, σ_1, and effective plastic strain, ϵ_p, on $\tilde{\sigma}_w$ which is expected to influence fracture predictions depending on the function Ψ_c. The following sections explore different forms of Ψ_c and their effect on the predictive capability of the modified Weibull stress in fracture toughness correlations for different specimen geometries with varying flow (hardening) properties.

3.2. Plausible forms for Ψ_c and the modified Weibull stress

A number of possibilities exist to introduce plastic strain effects on cleavage fracture based on different suppositions about which specific feature controls cleavage microcracking or the unstable propagation of a fully-formed, Griffith-like microcrack. Here, we consider four cases of interest for defining the function Ψ_c which have a direct bearing on the connection between the Weibull stress and macroscale fracture toughness: (1) exponential dependence of eligible microcracks on ϵ_p; (2) Limiting Distribution of Fracture Stress Using Particle Distribution; (3) the modified Beremin model incorporating plastic strain and (4) the influence of plastic strain on microcrack density.

3.2.1. Exponential dependence of eligible microcracks on ϵ_p

Recent extensions of the Beremin model made by Bordet et al. [58] have evolved to include plastic strain effects on cleavage fracture in terms of the probability for nucleating a carbide microcrack. Their original model considers that only freshly nucleated carbide particles, which become Griffith-like microcracks, are eligible to propagate unstably and, further, that the probability of microcrack nucleation, P_n, decreases as the number of uncracked carbides also decreases. While this could be assumed a reasonable assumption for small statistical samples, the number of (uncracked) carbides dispersed into the ferrite matrix in typical steels is plausibly very large so that, even if some uncracked carbides do become microcracks, there will still be a large number of left carbides which can become microcracks with increased plastic strain. In previous work, Hahn [30] pointed out that only a fraction of the largest and most favorably oriented carbides participate in the cleavage microcracking process, which is in contrast with the assumption of a direct dependence between cleavage microcracking and number of uncracked carbides as implied in the Bordet et al. approach [58].

Nevertheless, we may take a similar viewpoint and adopt a Poisson distribution [14,40,61] with parameter λ to define Ψ_c given by

$$\Psi_c = 1 - \exp(-\lambda\epsilon_p) \tag{11}$$

where λ can be interpreted as the average rate of fractured particles with size ℓ that become Griffith-like microcracks of size a with a small strain increment. Here, the underlying assumption is associated with a Poisson process [61] to describe the number of fractured particles that become eligible to propagate unstably thereby driving cleavage fracture.

Thus, the cleavage failure probability becomes

$$P_f(\sigma_1, \epsilon_p) = 1 - \exp\left\{-\frac{1}{V_0}\int_\Omega \left[1 - \exp(-\lambda\epsilon_p)\right]\cdot\left(\frac{\sigma_1}{\sigma_u}\right)^m d\Omega\right\} \tag{12}$$

from which the modified Weibull stress is written as

$$\tilde{\sigma}_w = \left\{\frac{1}{V_0}\int_\Omega \left[1 - \exp(-\lambda\epsilon_p)\right]\cdot\sigma_1^m d\Omega\right\}^{1/m} \tag{13}$$

3.2.2. Limiting distribution of fracture stress using particle distribution

To introduce a more detailed formulation for the cleavage failure probability, Wallin and Laukkanen (WL) [32], and earlier Wallin et al. [64], have argued that only a small number of all fractured particles actually contribute to the cleavage fracture process. Their approach allows incorporation of plastic strain effects on the cleavage fracture probability through the particle

fracture stress. Following similar arguments as those given in their work, we can derive the failure probability of cleavage fracture including effects of plastic strain as follows: let Ψ_c now be the fraction of fractured particles defined by WL [32] as a two-parameter Weibull distribution in the form

$$\Psi_c = 1 - \exp\left[-\left(\frac{\ell}{\ell_N}\right)^3 \cdot \left(\frac{\sigma_{pf}}{\sigma_{prs}}\right)^{\alpha_p}\right] \tag{14}$$

where ℓ is the particle size, ℓ_N represents a reference particle size, σ_{prs} is the particle's reference stress, α_p denotes the Weibull modulus and $\sigma_{pf} = \sqrt{1.3\sigma_1\epsilon_p E_d}$ characterizes the particle fracture stress in which σ_1 is the maximum principal stress, ϵ_p denotes the effective matrix plastic strain and E_d represents the particle's elastic modulus. Thus, assuming that a fractured particle with size ℓ becomes a Griffith-like microcrack with the same size and invoking the Poisson postulates outlined previously in Section 2.3 with the distribution of microcrack size described by Eq. (4), the elemental failure probability for the cracked body is expressed by

$$\delta P = \delta V \int_{\ell_c}^{\infty} \Psi_c \cdot g(\ell) d\ell = \frac{\delta V}{V_0} \int_{\ell_c}^{\infty} 1 - \exp\left[-\left(\frac{\ell}{\ell_N}\right)^3 \cdot \left(\frac{\sigma_{pf}}{\sigma_{prs}}\right)^{\alpha_p}\right] \cdot \left(\frac{\zeta_0}{\ell}\right)^{\zeta} d\ell \tag{15}$$

where the critical microcrack size, ℓ_c, is given as before by $\ell_c = K_{Ic}^2/(Y\sigma_1^2)$.

Using weakest link arguments, the above equation can be manipulated to derive the limiting distribution of cleavage fracture stress for the cracked body as

$$P_f(\sigma_1, \epsilon_p) = 1 - \exp\left\{-\frac{1}{V_0}\int_{\Omega}\int_{\ell_c}^{\infty} 1 - \exp\left[-\left(\frac{\ell}{\ell_N}\right)^3 \cdot \left(\frac{\sigma_{pf}}{\sigma_{prs}}\right)^{\alpha_p}\right] \cdot \left(\frac{\zeta_0}{\ell}\right)^{\zeta} d\ell d\Omega\right\} \tag{16}$$

where the dependence of P_f on σ_1 and ϵ_p through the particle fracture stress, σ_{pf}, and the critical microcrack size, ℓ_c, is readily understood.

The resulting expression for the cleavage failure probability cannot unfortunately be expressed in closed form for σ_1 and is solvable only by numerical methods. An approximate solution can be found if we make the assumption that the fraction of fractured particles defined by Eq. (14) is independent of the particle size, ℓ, so that the ratio $\ell/\ell_N \to 1$. Such may be formally justified by examining the nature of Eq. (14) more closely. WL [66] have pointed out that the fracture of particles dispersed in the ferrite matrix, such as carbides, exhibit a very brittle behavior and, therefore, can be characterized by a weakest link mechanism in connection with a statistical description of particle size effects. However, while their approach properly treats the potential effect of particle size on cleavage fracture, we favor a rather simpler procedure which allows direct comparison with the expressions for cleavage failure probability developed previously in Section 3.2. Further evaluations of Eq. (16) to predict effects of constraint on macroscopic measurements of fracture toughness are considered in the companion paper. Hence, accepting the present simplification, Eq. (16) resolves to

$$P_f(\sigma_1, \epsilon_p) = 1 - \exp\left[-\frac{1}{V_0}\int_{\Omega} 1 - \exp\left[-\left(\frac{\sqrt{1.3\sigma_1\epsilon_p E_d}}{\sigma_{prs}}\right)^{\alpha_p}\right] \cdot \left(\frac{\sigma_1}{\sigma_u}\right)^m d\Omega\right] \tag{17}$$

from which the modified Weibull stress now takes the form

$$\tilde{\sigma}_w = \left[\frac{1}{V_0}\int_{\Omega} 1 - \exp\left[-\left(\frac{\sqrt{1.3\sigma_1\epsilon_p E_d}}{\sigma_{prs}}\right)^{\alpha_p}\right] \cdot \sigma_1^m d\Omega\right]^{1/m}. \tag{18}$$

3.2.3. Modified Beremin model

Early work of the Beremin group [11] also recognized the potentially strong effects of plastic deformation on cleavage fracture. Based on experimental analyses of the failure strain for tensile notched specimens made of an ASTM A508 steel, they proposed a modified form of the previous Eq. (9) as

$$P_f(\sigma_1, \epsilon_p) = 1 - \exp\left[-\frac{1}{V_0}\int_{\Omega} \exp\left(-\frac{m\epsilon_p}{2}\right) \cdot \left(\frac{\sigma_1}{\sigma_u}\right)^m d\Omega\right] \tag{19}$$

with the Weibull stress defined by

$$\tilde{\sigma}_w = \left[\frac{1}{V_0}\int_{\Omega} \exp\left(-\frac{m\epsilon_p}{2}\right) \cdot \sigma_1^m d\Omega\right]^{1/m} \tag{20}$$

which indicates that $\tilde{\sigma}_w$ varies approximately with $\exp(-\epsilon_p/2)$.

Since $\Psi_c = \exp(-m\epsilon_p/2)$ in the above equation, observe the prominent role of the plastic strain at very low levels of ϵ_p (in which case $\Psi_c \to 1$) and a minimal effect for large values of ϵ_p such that $\Psi_c \to 0$. Moreover, the modified Beremin model is expected to give a good representation of the effects of plastic strain on fracture in the particular case of tensile loaded specimens from which the above expression for $\tilde{\sigma}_w$ was derived. While its application to predict effects of constraint in

fracture specimens remains relatively untested, it nevertheless provides a simple procedure to incorporate effects of plastic strain into the Weibull stress approach. This issue will be taken up in more detail in Section 5.2.

3.2.4. Influence of plastic strain on microcrack density

The procedures for determining a limiting form for the cleavage fracture stress discussed thus far have not explicitly considered the effects of plastic strain on the microcrack density. Previous fundamental work [22,23] clearly shows the strong effect of plastic deformation, in the form of inhomogeneous arrays of dislocations, on microcrack nucleation which triggers cleavage fracture at the material microlevel. Based upon direct observations of cleavage microcracking by plastic strain made in ferritic steels at varying temperatures [17–19], the microcrack density function given by Eq. (4) can then be further generalized in terms of

$$g(a) = \frac{\epsilon_p^{\beta}}{V_0}\left(\frac{\varsigma_0}{a}\right)^{\zeta} \tag{21}$$

where ϵ_p is the (effective) plastic strain and β represents a parameter defining a power law relationship between the microcrack density and plastic strain as inferred in Lindley et al. [18]. Further, parameter β defines the contribution of the plastic strain on cleavage fracture probability; for example, setting $\beta = 0$ recovers the conventional description for the probability distribution of fracture stress whereas $\beta = 1$ reflects a linear dependence of microcrack density on plastic strain. Again, the equivalence $g(a) \leftrightarrow g(\ell)$ is readily understood thereby implying that an increase in plastic strain affects the number of fractured particles with size ℓ which become Griffith-like microcracks with size a and thereby does not alter the shape of the microflaw distribution defined by parameter ς.

Now, upon introducing Eq. (21) into Eq. (3) and following the same development as in Section 2.3, the probability distribution for the fracture stress of a cracked solid with increased levels of loading yields

$$P_f(\sigma_1, \epsilon_p) = 1 - \exp\left[-\frac{1}{V_0}\int_{\Omega} \epsilon_p^{\beta} \cdot \left(\frac{\sigma_1}{\sigma_u}\right)^m d\Omega\right] \tag{22}$$

where it is understood that $\Psi_c(\epsilon_p) = \epsilon_p^{\beta}$. Thus, the modified Weibull stress becomes

$$\tilde{\sigma}_w = \left[\frac{1}{V_0}\int_{\Omega} \epsilon_p^{\beta} \cdot \sigma_1^m d\Omega\right]^{1/m}. \tag{23}$$

The above plastic term correction simply describes the change in cleavage fracture probability that results from the growth in microcrack density with increased levels of near-tip plastic strain. Observe, however, that this form of Ψ_c does not provide an exact description for the fraction of microcracks nucleated inside the near-tip fracture process zone with increased deformation which are eligible to propagate unstably. It nevertheless gives an alternative way of incorporating plastic strain effects into the Weibull stress formulation by changing the microcrack density function rather than the number of eligible microcracks. Similar approaches adopting the same viewpoint of a functional form between microcrack density and plastic strain include the works of Kroon and Faleskog [67], Gao et al. [60] and Ruggieri [21].

4. Computational models and finite element procedures

4.1. MBL model

The modified boundary layer (MBL) model illustrated in Fig. 3(a), originally proposed by Rice [68], consists of a (very large) circular region containing an edge crack. With the plastic region limited to a small fraction of the domain radius, $R_p < R/20$ where R_p is the radius (size) of the crack-tip plastic zone, the general form of the asymptotic crack-tip stress fields well outside the plastic region is given by William's expansion [69] as

$$\sigma_{ij} = \frac{K_I}{\sqrt{2\pi r}} f_{ij}(\theta) + T\delta_{1i}\delta_{1j} \tag{24}$$

where K_I is the elastic stress intensity factor, f_{ij} define the angular variations of in-plane stress components, (r, θ) are polar coordinates centered at the crack tip (see Fig. 3(a)) and the non-singular term represents a tension (or compression) stress parallel to the crack. Numerical solutions for different levels of parameters $(K_I, T/\sigma_0)$ are generated by imposing the corresponding displacements of the elastic, Mode I singular field on the outer circular boundary $(r = R)$ which encloses the crack [70].

The plane-strain SSY analyses employ a conventional mesh configuration having a focused ring of elements surrounding the crack front. This SSY model has a single unit thickness layer $(B = 1$ mm$)$ of 2065 8-node, 3-D elements. To achieve plane-strain conditions for the current study, the single thickness layer of the 3-D elements is defined with out-of-plane displacements constrained to vanish $(w = 0)$ on the nodes. A small initial root radius at the crack tip (blunt tip) is employed to enhance convergence of the nonlinear iterations as presented in Fig. 3(a); the radius of the blunt tip, ρ_0, is 0.0025 μm with $R/\rho_0 = 10^6$. To limit effects of the initial root radius on the crack-tip stresses, the CTOD (δ) is required to equal four times the initial radius (ρ_0) at a deformation consistent with $(b\sigma_0/J) = 250$, where σ_0 is the reference yield stress and b is the

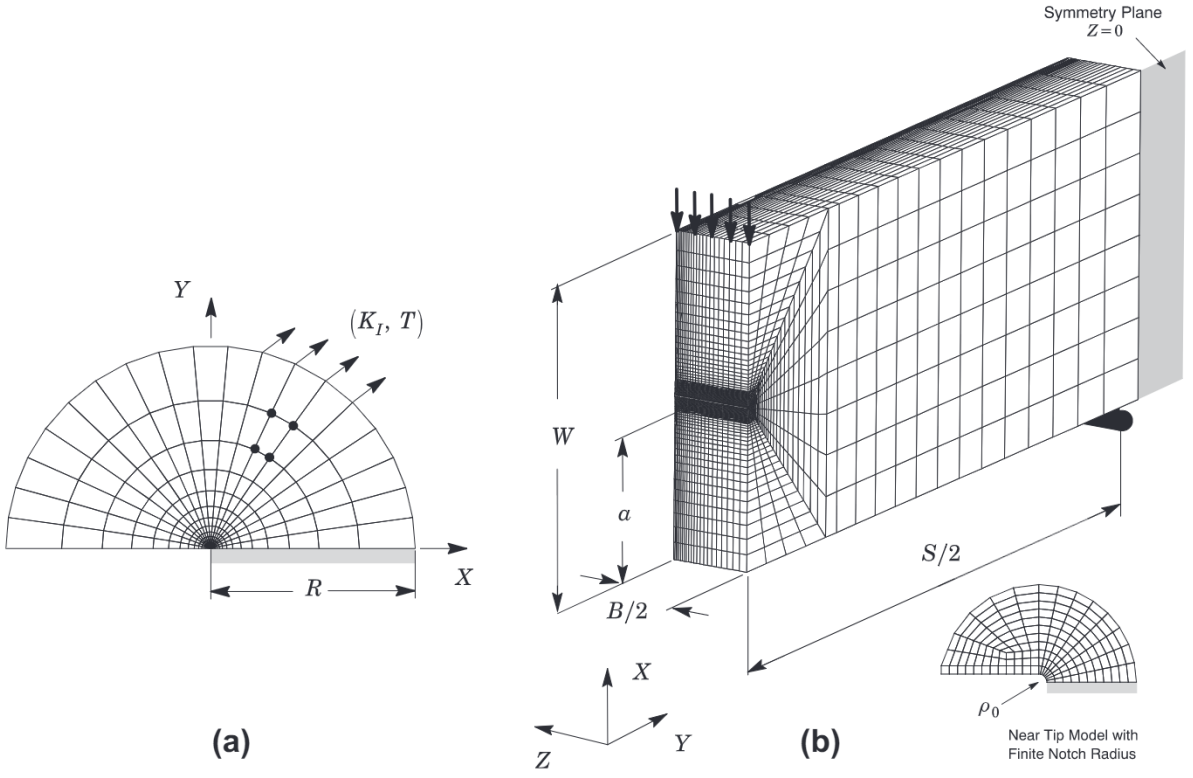

Fig. 3. (a) Definition of the modified boundary layer (MBL) problem; (b) quarter-symmetric finite element model for the deeply-cracked 1-T SE(B) specimen with $a/W = 0.5$.

remaining crack ligament. This condition requires $\rho_0 = 0.0025$ mm for SSY model and flow properties considered in this work. A series of SSY analyses containing a range of initial root radii confirm that the near-tip stresses after reaching steady state conditions become independent of the initial root radius for $\delta/\rho_0 > 4$ [71].

4.2. SE(B) fracture specimens

Nonlinear numerical analyses are conducted on 3-D finite element models for plane-sided 1T SE(B) fracture specimens ($B = 25$ mm) with conventional geometry ($W = 2B$ and $S = 4W$) and varying crack sizes characterized by $a/W = 0.5$ and 0.2. Here, a denotes the crack length, B is the specimen thickness, W defines the specimen width and S represents the specimen span.

Fig. 3(b) shows a typical finite element model constructed for analyses of the deeply cracked SE(B) specimen with $a/W = 0.5$. The numerical model for the shallow crack SE(B) specimen with $a/W = 0.2$ has very similar features. Geometric and loading symmetry about the crack plane ($Y = 0$) and the longitudinal midplane ($Z = 0$) enables the use of one-quarter models as indicated with appropriate constraints imposed on the symmetry planes. A conventional mesh configuration having a focused ring of elements surrounding the crack front is used with a small key-hole at the crack tip and sufficient refinement near the tip to provide adequate resolution of the stress fields; the radius of the key-hole, ρ_0, is 10 μm (0.01 mm). Use of a small initial root radius at the crack front (blunt tip) provides two numerical benefits: (1) it accelerates convergence of the finite-strain plasticity algorithms during the initial stage of blunting, and (2) it minimizes numerical problems during computation of the Weibull stress over material incident on the crack tip.

The mesh has 32 variable thickness layers defined over the half-thickness ($B/2$); the thickest layer is defined at $Z = 0$ with thinner layers defined near the stress-free surface ($Z = B/2$) to accommodate strong Z variations in the stress distribution. Here, the layer thickness at the specimen midplane ($Z = 0$) is $0.04B$ whereas the layer defined near the free surface ($Z = B/2$) is $0.004B$. By using this level of mesh refinement over the half-thickness (and, thus, over the half-crack front), the numerical models fully capture the 3-D crack front stress fields thereby describing more accurately the evolution of $\bar{\sigma}_w$ with increased loading addressed later in Section 5.2. The quarter-symmetric, 3-D model for this specimen has approximately 36200 nodes and 32500 8-node isoparametric elements. These finite element models are loaded by displacement increments imposed on the top nodes for the symmetry plane to enhance numerical convergence with increased loading and plastic deformation.

4.3. Material models and solution procedures

The numerical solutions described here utilize an elastic–plastic constitutive model with J_2 flow theory and conventional Mises plasticity in large geometry change (LGC) setting. The numerical solutions employ a simple power-hardening model to characterize the uniaxial true ($\bar{\sigma}$) stress *vs.* logarithmic strain ($\bar{\epsilon}$) in the form

$$\frac{\bar{\epsilon}}{\epsilon_0}=\frac{\bar{\sigma}}{\sigma_0}, \quad \bar{\epsilon}\leqslant\epsilon_0; \quad \frac{\bar{\epsilon}}{\epsilon_0}=\left(\frac{\bar{\sigma}}{\sigma_0}\right)^n, \quad \bar{\epsilon}>\epsilon_0 \tag{25}$$

where σ_0 and ϵ_0 are the reference (yield) stress and strain, and n denotes the strain hardening exponent. The finite element analyses consider material flow properties covering typical structural, pressure vessel and pipeline grade steels with $E=206$ GPa and $\nu=0.3$: $n=5$ and $E/\sigma_0=800$ (high hardening material), $n=10$ and $E/\sigma_0=500$ (moderate hardening material), $n=20$ and $E/\sigma_0=300$ (low hardening material). These ranges of properties also reflect the upward trend in yield stress with the increase in strain hardening exponent, n, characteristic of ferritic structural steels, including pressure vessel steels.

The finite element code WARP3D [72] provides the numerical solutions for the plane-strain and 3-D analyses reported here. Evaluation of the J-integral derives from a domain integral procedure [73] which yields J-values retaining strong path independence for domains defined outside the highly strained material near the crack tip. For the 3D analyses reported in Section 5.2, a thickness average value for J is computed over domains defined outside the material having the highly non-proportional histories of the near-tip fields.

In the present methodology, a requisite feature to obtain nearly invariant $\tilde{\sigma}_w$-values at a fixed, specified macroscopic loading (as characterized by J) is to generate converged numerical descriptions of the crack-tip stress fields which are accurate over distances of order a few CTODs. A weak, implicit length-scale enters the finite element computations through the near-tip mesh size. For example, insufficient mesh refinement reduces peak stress values ahead of the crack front, especially at smaller load levels, thereby strongly affecting the compute values of $\tilde{\sigma}_w$ – recall the Weibull stress calculation involved the principal stress raised to a large power defined by the Weibull modulus. The plane-strain and 3-D models used in this study possess the required level of mesh refinement to resolve accurately the crack-tip stress and strain to compute nearly invariant $\tilde{\sigma}_w$-values.

4.4. Numerical evaluation of crack front stress triaxiality

To illustrate the effects of specimen geometry on crack-tip constraint and implications for the toughness ratios of SE(B) specimens derived from the modified Weibull stress addressed in Section 5.2, the present study adopts the $J-Q$ methodology [7,8] to characterize the crack front stress fields with increased specimen deformation. Here, we present only the salient features of the methodology. Readers are referred to the work of Dodds et al. [3] and Nevalainen and Dodds [70] for details.

O'Dowd and Shih (OS) [7,8] introduced an approximate two-parameter description for the elastic–plastic crack tip fields based upon a triaxiality parameter more applicable under large scale yielding (LSY) conditions for materials with elastic–plastic response described by a power hardening law given by $\epsilon/\epsilon_0\propto(\sigma/\sigma_0)^n$. Here, n denotes the strain hardening exponent, σ_0 and ϵ_0 are the reference (yield) stress and strain, respectively. Guided by detailed numerical analyses employing a modified boundary layer (MBL) model, OS defined the difference field relative to a high triaxiality reference stress state in terms of a hydrostatic parameter in the form of

$$Q\equiv\frac{(\sigma_{yy})_{FB}-(\sigma_{yy})_{SSY}}{\sigma_0} \tag{26}$$

where the difference field described in terms of the opening (Mode I) stresses, σ_{yy}, is conventionally evaluated at the normalized crack-tip distance $\bar{r}=r/(J/\sigma_0)=2$. Here, it is readily understood that the dimensionless parameter Q defines the amount by which σ_{ij} in fracture specimens, $(\sigma_{ij})_{FB}$, differ from the adopted high triaxiality reference SSY solution, $(\sigma_{ij})_{SSY}$. As will be shown in Section 5.2, construction of $J-Q$ trajectories for the analyzed fracture specimens then follows by evaluation of Eq. (26) at each stage of loading in the finite body. The research code Fractus2D [74] is employed to compute the $J-Q$ curves for each fracture specimen shown in Section 5.2.

5. Results from the parameter analysis

The following sections provide selected key results derived from the numerical analyses conducted on the small-scale yielding model under varying levels of T-stress and on the SE(B) specimens used to assess effects of crack-tip constraint and specimen geometry on the modified Weibull stress incorporating plastic strain effects. Within the present context, the Weibull stress is interpreted as a local crack driving force which describes the microstructural process of cleavage fracture, thus allowing comparisons of $\tilde{\sigma}_w$-trajectories with increased deformation and varying forms for the function Ψ_c. The presentation begins with a small scale yielding description of the various forms of plastic strain effects on the evolution of $\tilde{\sigma}_w$ with J derived from the MBL model. These SSY analyses provide insights into the quantitative effects of key plastic

strain parameters (which are related to the function Ψ_c) on the modified Weibull stress, $\tilde{\sigma}_w$. The variation of macroscale crack driving force (J) resulting from constraint loss in the 3-D SE(B) models is then characterized in terms of the toughness scaling model based upon $\tilde{\sigma}_w$. Primary attention is given to examining the significance of the function Ψ_c on constraint correlations of J-values in deep and shallow crack SE(B) geometries. Using the Weibull stress concept, these analyses permit establishing fracture toughness ratios for high and low constraint fracture specimens.

For most of the calculations that follow, the values of the key parameters defining the function Ψ_c are dictated in part by the previous exploratory studies of Ruggieri and Dodds [75] on cleavage fracture predictions for a pressure vessel steel. Specifically, while the choices of parameter λ describing the exponential dependence on ϵ_p and the Weibull modulus, α_p, defining the particle fracture stress distribution adopted here are somewhat arbitrary, they are nevertheless consistent with their preliminary predictions of constraint effects on measured fracture toughness in small-sized fracture specimens.

5.1. Weibull stress trajectories under SSY conditions

Small-scale yielding solutions with varying levels of applied T-stress are generated for power-law hardening materials having three levels of strain hardening: $n = 5$ $(E/\sigma_0 = 800), n = 10$ $(E/\sigma_0 = 500)$ and $n = 20$ $(E/\sigma_0 = 300)$. In each analysis, the full value of T-stress is imposed first (which causes no yielding), followed by the K-field (or, equivalently, the elastic J-field) imposed in an incremental manner. Evaluation of the Weibull stress, $\tilde{\sigma}_w$, under increased levels of macroscopic loading is performed by setting $m = 20$ in Eq. (10); this value for the Weibull modulus has been chosen to characterize the distribution of Weibull stress at cleavage fracture for a nuclear pressure vessel steel (ASTM A508) with moderate hardening properties [11]. Several previous works, including those of Minami et al. [51], Ruggieri and Dodds [52] and Gao et al. [76] among others, provide calibrated m-values in the range of $10 \sim 20$ for ferritic structural steels.

Before launching into a comparison of the varying forms of $\tilde{\sigma}_w$ incorporating effects of plastic strain, it is useful to briefly address the influence of key parameters related to the function Ψ_c which have a direct bearing on the computed Weibull stress trajectories. These analyses are conducted for the SSY problem with $T/\sigma_0 = 0$ and the moderate hardening material ($n = 10$). The trends resulting from this study are essentially similar for other hardening properties and T-stress levels; to conserve space, those results are not included here.

Fig. 4 compares the evolution of $\tilde{\sigma}_w/\sigma_0$ with increased loading for the microcrack density model incorporating effects of plastic strain defined by Eq. (23) with five different values of β: 0, 0.5, 1.0, 2.0 and 3.0. In particular, the $\beta = 1$ value reflects a linear dependence of microcrack density on plastic strain which is in accord with the experimental observations of Lindley et al. [18] and Gurland [19] as well as previous studies conducted by Kroon and Faleskog [67], Gao et al. [60] and Ruggieri [21]. Further, recall that $\beta = 0$ simply recovers the conventional Weibull stress model defined by Eq. (7). These analyses show a rather strong sensitivity of $\tilde{\sigma}_w$ to the functional form of the plastic strain term defined by Eq. (22). For a fixed level of loading, as characterized by J/σ_0, a decrease in β increases the computed Weibull stress. This behavior can be understood by examining Eq. (21) defining the microcrack density function. Clearly, when $\beta \to 0$ (in which case the modified Weibull stress form approaches the conventional Beremin expression), the number of microcracks per unit volume which are eligible to propagate unstably increases thereby increasing the value of $\tilde{\sigma}_w$ (here, interpreted as an effective crack driving force in the present context).

Fig. 5 shows the normalized Weibull stress trajectories for the exponential dependence model with varying λ-values: 0.1, 0.2, 0.3, 0.5 and 1. Since parameter λ represents the average rate of fracture particles that become eligible to propagate unstably with a small plastic strain increment, it is plausible to assume for the present investigation that λ varies between 0 (*i.e.*, $P_f = 0$) and 1 thereby providing justification to the adopted range of values and, at the same time, making contact with previous exploratory analyses of Ruggieri and Dodds [75]. Work in progress addresses in more detail the effects of parameter λ on fracture toughness predictions for a pressure vessel steel. To facilitate comparisons, this plot also includes results for the

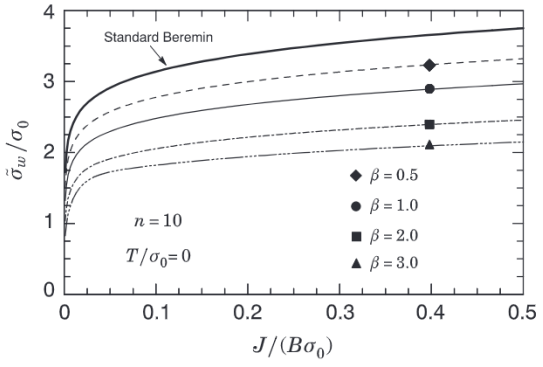

Fig. 4. Evolution of $\tilde{\sigma}_w/\sigma_0$ with increased loading for the microcrack density model incorporating effects of plastic strain with five different values of β: 0, 0.5, 1.0, 2.0 and 3.0.

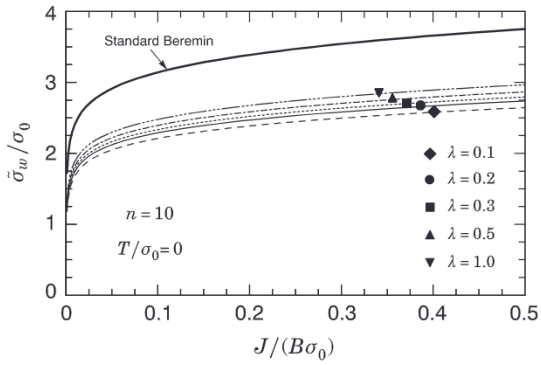

Fig. 5. Normalized Weibull stress trajectories for the microcrack nucleation model with varying λ-values: 0.1, 0.2, 0.3 and 0.5.

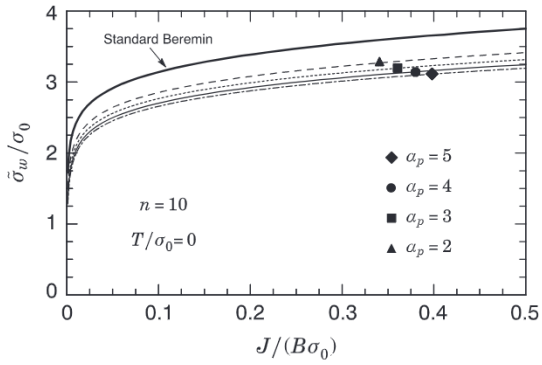

Fig. 6. Computed curves for $\tilde{\sigma}_w/\sigma_0$ with increased loading for the simplified particle distribution model with $\alpha_p = 2$, 3, 4 and 5 ($\sigma_{prs} = 6000$ MPa and $E_d = 400$ GPa).

conventional Weibull stress model. The relatively minor role of parameter λ in the analyzed range is evident in the results displayed in Fig. 5. For the λ-values considered in these analyses, the normalized Weibull stress, $\tilde{\sigma}_w/\sigma_0$ increases only slightly from $\lambda = 0.1$ to $\lambda = 1.0$.

Fig. 6 displays the computed curves for $\tilde{\sigma}_w/\sigma_0$ with increased loading derived from the simplified particle distribution defined by Eq. (18) for $\alpha_p = 2$, 3, 4 and 5 and holding other parameters fixed by setting $\sigma_{prs} = 6000$ MPa (yield stress of the particle) and $E_d = 400$ GPa (elastic modulus of the particle). These values are consistent with previous analysis by Wallin and Laukkanen [32] and correspond to typical fracture stress values for iron carbide particles (cementite). Again, the conventional Weibull stress model is included in the plot to facilitate comparisons. The Weibull stress trajectories depend weakly on α_p; here, a decrease in α_p results in slight increase of the computed Weibull stress. In particular, the value $\alpha_p = 4$ also agrees with the investigation pursued by Wallin and Laukkanen [32] who also compared their adopted particle distribution with experimental fractography.

We now present a comparison between the conventional Beremin model described by Eq. (5) and the modified Weibull stress approach making use of varying forms of $\tilde{\sigma}_w$ incorporating effects of plastic strain: (1) dependence of microcrack density on plastic strain with $\beta = 1$; (2) exponential dependence model with $\lambda = 0.2$, and (3) simplified particle distribution (WL model) with $\alpha_p = 4, \sigma_{prs} = 6000$ MPa and $E_d = 400$ GPa. As already anticipated, these choices are consistent with the previous exploratory analyses of Ruggieri and Dodds [75] on cleavage fracture predictions for a pressure vessel steel. Fig. 7(a)–(b) displays Weibull stress trajectories generated under increased loading for the $n = 10$ material and two widely different values of T-stress defined by $T/\sigma_0 = 0$ and $T/\sigma_0 = -0.5$. Fig. 8(a)–(b) provides the variation of $\tilde{\sigma}_w$ with increased loading for $T/\sigma_0 = 0$ and two different hardening materials described by $n = 5$ (high hardening) and $n = 20$ (low hardening). The significant features include: (1) the magnitudes of the normalized Weibull stress for the standard Beremin model (*i.e.*, without considering effects of plastic strain) are larger than the analyzed forms of $\tilde{\sigma}_w$ for any value of T-stress; note that such results could be anticipated from the discussion presented in Section 3 as the number of eligible microcracks for the standard Beremin model is larger than for the varying forms of $\tilde{\sigma}_w$ incorporating effects of plastic strain; (2) for the adopted set of strain parameters, the exponential dependence model provides the lowest $\tilde{\sigma}_w$-curves whereas the simplified particle distribution model yields the highest Weibull stress trajectories; (3) the Weibull stress trajectories also scale approximately with hardening properties; here, high strain hardening ($n = 5$) increases the magnitudes of $\tilde{\sigma}_w/\sigma_0$ relative to other hardening materials (observe that the scale in Fig. 8(a) is different).

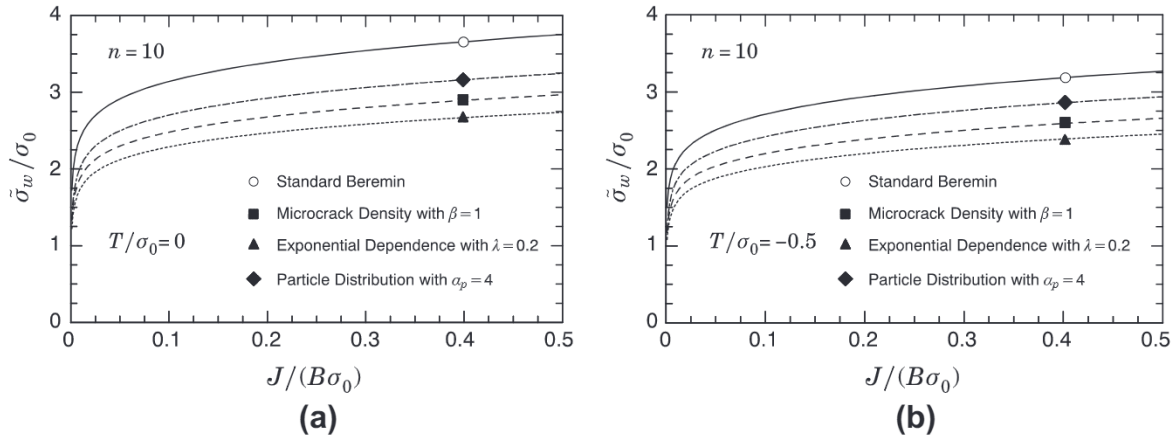

Fig. 7. Weibull stress trajectories, $\tilde{\sigma}_w/\sigma_0$, generated under increased loading for the $n = 10$ material and two widely different values of T-stress: (a) $T/\sigma_0 = 0$ and (b) $T/\sigma_0 = -0.5$.

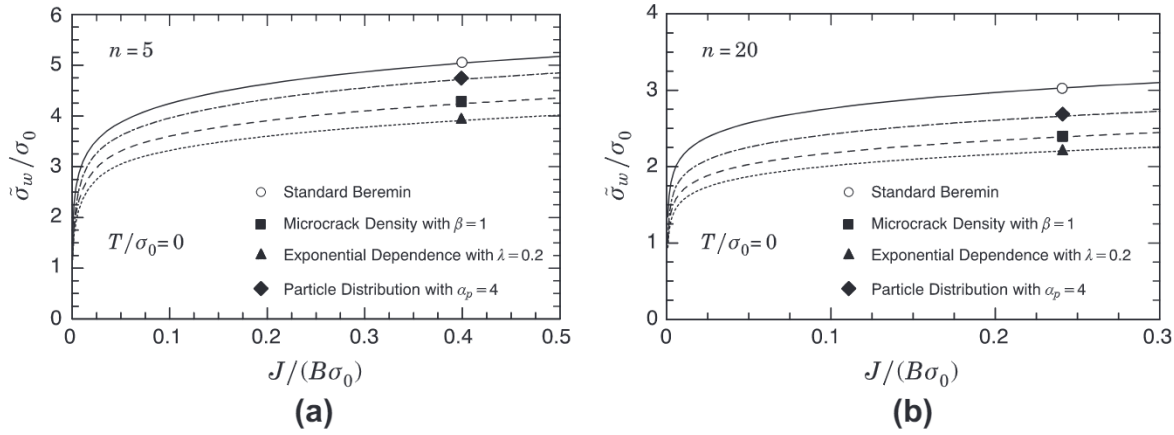

Fig. 8. Variation of $\tilde{\sigma}_w$ with increased loading for $T/\sigma_0 = 0$ and two different hardening materials: (a) $n = 5$ and (b) $n = 20$.

5.2. Effects of plastic strain on toughness ratios for SE(B) fracture specimens

While the previous small-scale yielding results show general characteristics of the modified Weibull stress model incorporating plastic strain effects, more specific features related to the predictive capability of the present probabilistic formulation can be studied through recourse to a toughness scaling methodology (TSM) based upon $\tilde{\sigma}_w$. Moreover, a number of previous works have demonstrated a strong interaction between in-plane and through-thickness effects on crack-front fields not captured in the plane-strain analyses (see, *e.g.*, Nevalainen and Dodds [70]). Thus, while plane-strain models give gross features of effects of plastic strain on toughness ratios for the analyzed SE(B) specimens, some of the detailed features of the coupling between in-plane and through-thickness effects on $\tilde{\sigma}_w$ can be studied through recourse to full 3-D analysis.

5.2.1. 3-D constraint effects in SE(B) specimens

This section briefly examines the constraint loss phenomenon and the coupling nature of in-plane and through-thickness effects on crack front fields in the SE(B) specimens with the $n = 10$ material. Similar results are found for other material properties but they are not shown here in interest of space. Fig. 9(a) displays the distribution of near-tip opening stresses, σ_{yy}, at the same level of applied loading, $J = 200$ kJ/m^2, for the deep and shallow crack SE(B) models extracted at the specimen centerplane ($Z = 0$) – refer to Fig. 3(b). The distribution of the out-of-plane stresses, σ_{zz}, over the crack front for two widely differing load levels, $J = 100$ and 200 kJ/m^2 is shown in Fig. 9(b); here, the σ_{zz} stresses are extracted at the normalized crack-tip distance, $r/(J/\sigma_0) = 2$, which corresponds approximately to 3 × CTOD [2]. In these plots, the opening stresses are normalized by the material yield stress, σ_0, and crack-tip distances are normalized by J/σ_0. The plane-strain SSY field (corresponding to the MBL solution described previously in Section 4.1) is also included in Fig. 9(a) for reference. As could be expected, the deeply-cracked specimen exhibits higher opening stresses at the same J-value in comparison with the shallow

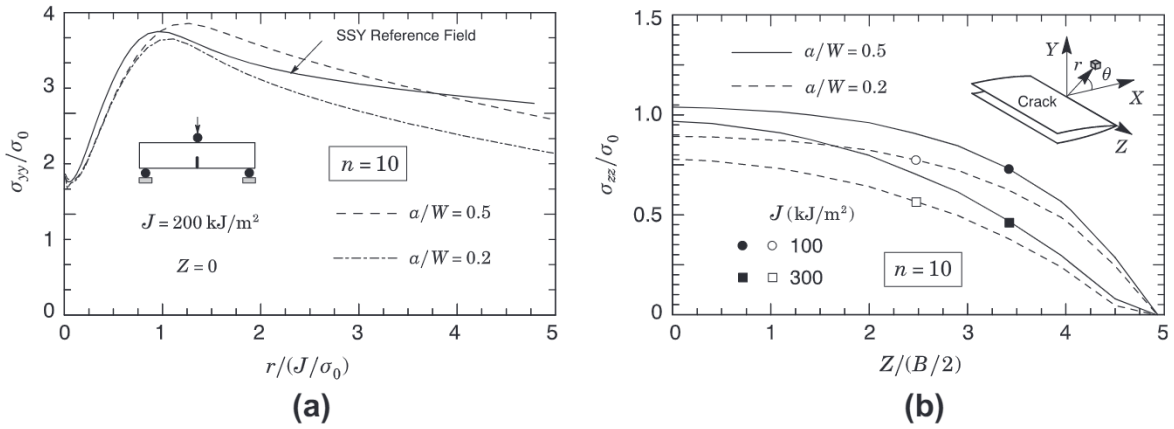

Fig. 9. Crack-tip stress distributions for the SE(B) specimens with the $n = 10$ material: (a) variation of near-tip opening stresses (σ_{yy}) with normalized crack-tip distance at the specimen center plane ($Z = 0$) and $\theta = 0$; (b) variation of out-of-plane stresses (σ_{zz}) over the crack front at the normalized crack-tip distance, $r/(J/\sigma_0) = 2$.

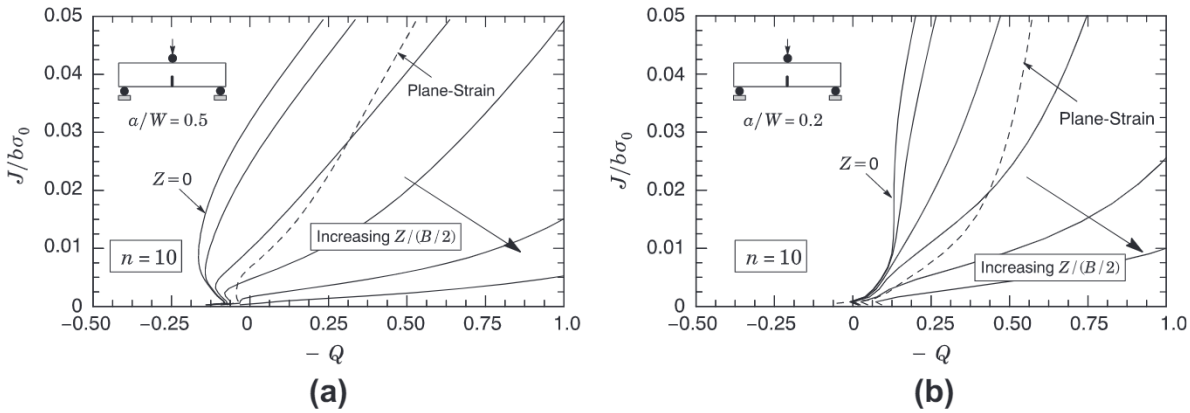

Fig. 10. $J - Q$ trajectories for the SE(B) specimens with the $n = 10$ material at several crack front locations: (a) $a/W = 0.5$; (b) $a/W = 0.2$.

crack geometry. The distribution of σ_{zz} over the crack front shown in Fig. 9(b) reveals maximum values over a large fraction of the specimen thickness extending from midplane and then gradually decreasing as the stress-free surface is approached. In every case under consideration, the stresses for the shallow crack specimens relax below the values corresponding to the high constraint, deeply cracked bend configuration.

Fig. 10 displays the effects of specimen geometry on the $J - Q$ trajectories at selected locations along the crack front for the SE(B) specimens with the $n = 10$ material. In the present analyses, construction of the $J - Q$ trajectories is conducted at locations along the crack front which correspond to the center of each layer in the finite element model as given by the non-dimensional parameter $Z/(B/2)$. The first layer is defined at $Z = 0$ which represents the mid-thickness of the specimen. For comparison, the plane-strain results corresponding to each specimen geometry are also included in the plots. Again, essentially similar results are found for other material properties but they are not shown here to conserve space.

The trends are clear. The evolution of Q as loading progresses depends markedly on the location along the crack front and on the specimen geometry. Not surprisingly, the crack front locations maintaining the highest constraint are on the mid-thickness region ($Z = 0$). Observe, however, that the levels of crack-tip constraint at front locations within the mid-thickness region for the deeply cracked specimen specimens are much higher than the corresponding levels for the shallow crack geometry for most of the deformation range. Such results follow similar trends obtained in previous work of Nevalainen and Dodds [70] and Silva et al. [77]. The remarkable range of crack-tip constraint along the crack front for each specimen geometry makes correlation of fracture toughness across these crack configurations a rather complex task thereby providing additional support for the analysis of toughness ratios in SE(B) specimens based on the modified Weibull stress discussed next.

5.2.2. Dependence of toughness ratios on plastic strain

The TSM proposed earlier by Dodds and Anderson [78,79] and later by Ruggieri and Dodds [52], here generalized to include plastic strain effects, assumes equal cleavage failure probability at a specified value of $\tilde{\sigma}_w$ across different crack configurations even though the loading parameter (measured by J in the present work) may vary widely due to constraint loss.

The 3-D finite element analyses of deep and shallow crack SE(B) fracture specimens provides a basis to assess the significance of Ψ_c on constraint correlations of macroscopic crack driving forces described by J. Here, we address the effects of plastic strain on toughness ratios based on the modified Weibull stress, $\tilde{\sigma}_w$, incorporating various forms of Ψ_c: (1) standard Beremin model in which $\Psi_c = 1$; (2) modified Beremin model; (3) dependence of microcrack density on plastic strain with $\beta = 1$ and 2; (4) exponential dependence on ϵ_p with $\lambda = 0.2$, and (5) simplified particle distribution (WL model) with $\alpha_p = 4, \sigma_{prs} = 6000$ MPa and $E_d = 400$ GPa.

Fig. 11(a)–(f) provides the constraint correlations ($J_{SEB}^{a/W=0.2} \rightarrow J_{SEB}^{a/W=0.5}$) for the $n = 10$ material and varying plastic strain models with different Weibull moduli, m. The present computations consider values of $m = 5$, 10, 15 and 20 to assess the sensitivity of constraint correlations on the specified Weibull modulus. These m-values are consistent with previously reported values for structural steels. Each curve provides pairs of J-values in the shallow and deep crack SE(B) specimens

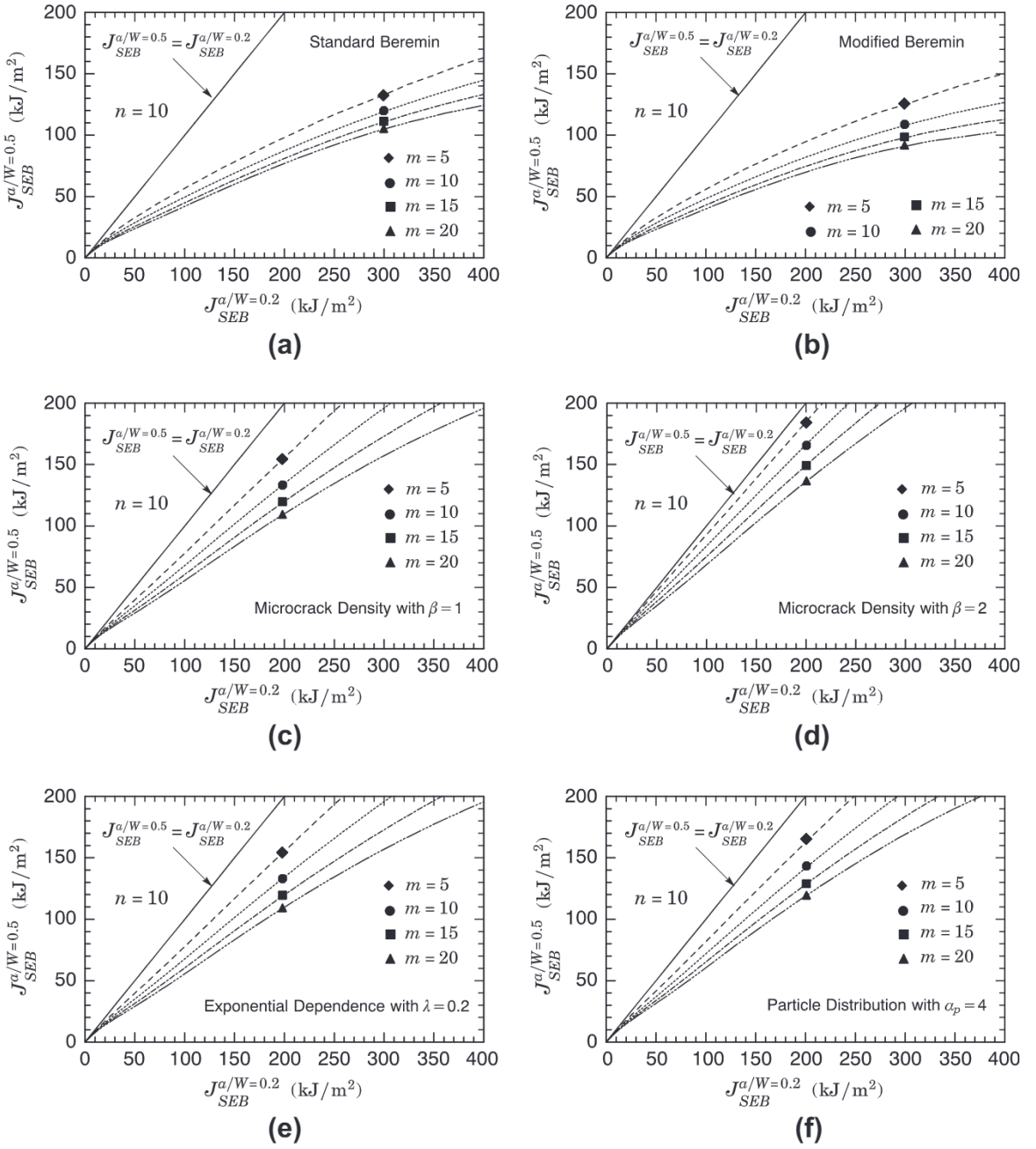

Fig. 11. Constraint correlations of J-values for the $n = 10$ material and varying plastic strain models with different Weibull moduli, m.

which produce the same Weibull stress, $\tilde{\sigma}_w$, for a fixed m-value. Further, within the present context of probabilistic fracture mechanics, each pair $(J_{SEB}^{a/W=0.2}, J_{SEB}^{a/W=0.5})$ on a given m-curve defines equal failure probabilities for cleavage fracture. A reference line is shown which defines a unit toughness ratio defined by $J_{SEB}^{a/W=0.2} = J_{SEB}^{a/W=0.5}$. For each value of the Weibull modulus, the shallow crack specimen and deeply cracked configuration agree very well early in the loading history while the specimens maintains near SSY conditions across the crack front with essentially identical near-tip stresses and fracture process zone sizes. Once near-front stresses deviate from the (plane-strain) SSY levels, the curves for the shallow crack SE(B) specimens fail to increase at the same rate with further loading thereby clearly showing the gradual nature of constraint loss in the shallow crack SE(B) specimens with increased loading. The Weibull modulus does have an appreciable effect on the resulting toughness ratios for the deep and shallow crack bend configurations. Here, smaller m values indicate a higher load level at the onset of constraint loss and reduced toughness ratios for these specimen geometries – larger m values assign a greater weight factor to stresses at locations very near the crack front.

The effect of plastic strain on the constraint correlations resulting from the proposed methodology is amply demonstrated by the results in Fig. 11. Compared with the standard Beremin model, inclusion of plastic strain effects as shown in Fig. 11(c-f) reduces the amount of constraint correction defined by the ratio $J_{SEB}^{a/W=0.2}/J_{SEB}^{a/W=0.5}$. Since Ψ_c changes with ϵ_p when the modified Weibull stress, $\tilde{\sigma}_w$, is defined by Eqs. (23), (13) and (18), the relative position of the $\tilde{\sigma}_w - J$ curve for the shallow crack specimen shifts closer to the corresponding curve for the deep crack specimen thereby reducing the ratio $J_{SEB}^{a/W=0.2}/J_{SEB}^{a/W=0.5}$. In contrast, the modified Beremin model slightly increases the constraint correction ratios for all m-values. Here, as already mentioned before, $\Psi_c \to 0$ with increased values of ϵ_p thereby shifting the relative position of the $\tilde{\sigma}_w - J$ curve for the shallow crack specimen farther.

Figs. 12 and 13 display constraint correlations of J-values for the high hardening $(n = 5)$ and low hardening $(n = 20)$ materials with varying Weibull moduli, m, and selected functions, Ψ_c, including the standard Beremin model. The rather strong dependence of the toughness ratios on strain hardening behavior for the deep and shallow crack bend specimens is evident in these plots. Consider first the constraint correlations for the high hardening material $(n = 5)$ and varying Weibull moduli, m. The salient features associated with these results include: (1) the effects of constraint loss on J-values for the shallow crack specimen are relatively small resulting in toughness ratios in the range $J_{SEB}^{a/W=0.2} = 1.2 \sim 1.3 \cdot J_{SEB}^{a/W=0.5}$; (2) the toughness ratios depend weakly on the Weibull modulus in the range $5 \leqslant m \leq 20$ and (3) the toughness ratios are relatively

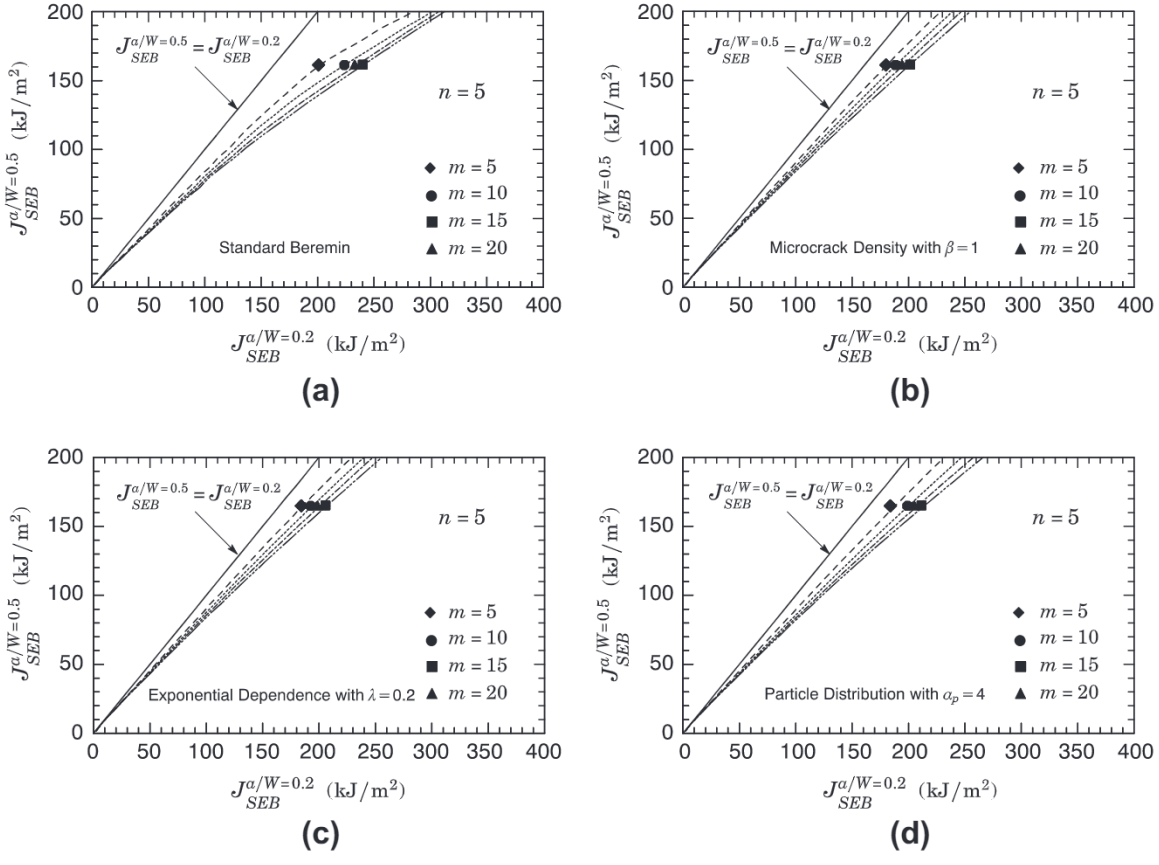

Fig. 12. Constraint correlations of J-values for the $n = 5$ material and varying plastic strain models with different Weibull moduli, m.

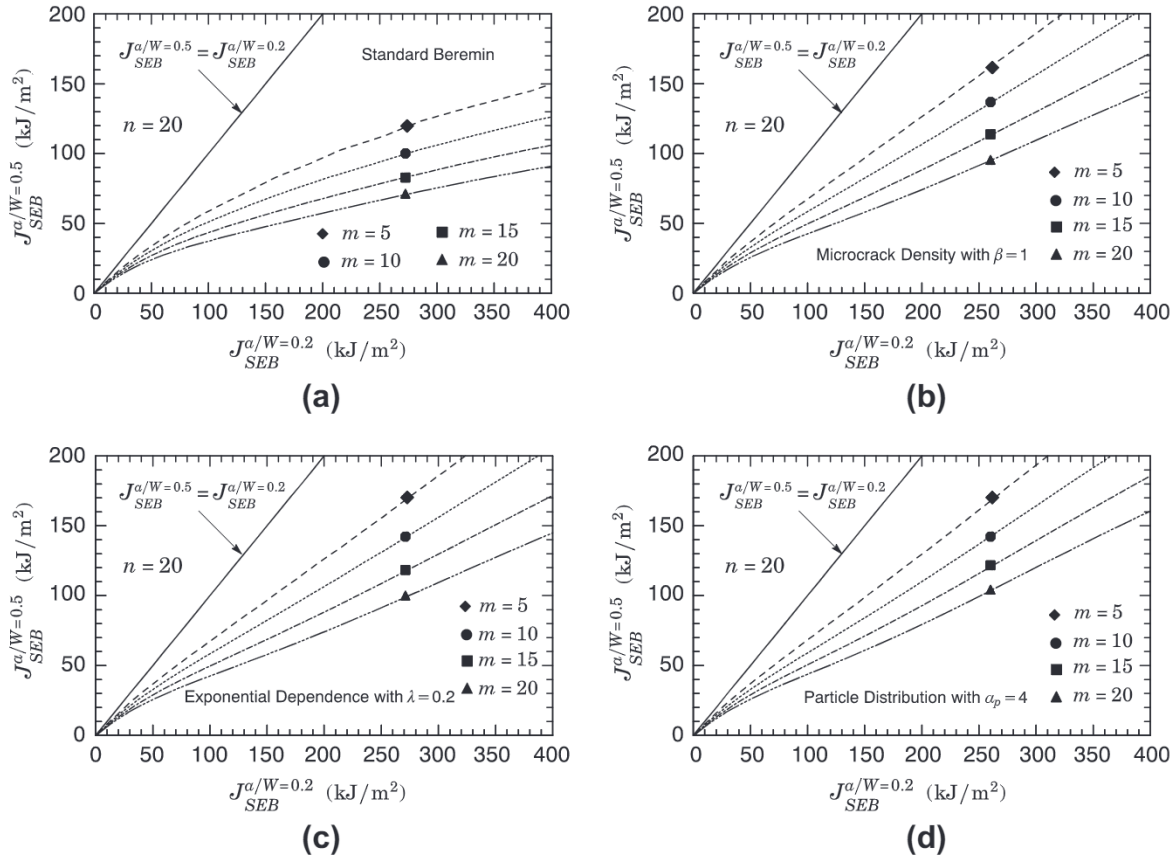

Fig. 13. Constraint correlations of J-values for the $n = 20$ material and varying plastic strain models with different Weibull moduli, m.

insensitive to the adopted function Ψ_c when plastic strain effects are considered. This behavior is consistent with the strong hardening capacity of the material which suppresses development of large near-tip plastic strains thereby affecting weakly $\tilde{\sigma}_w$. Now, direct attention to the constraint correlations for the low hardening material ($n = 20$) and different Weibull moduli, m. Here, a strong effect of constraint loss on the J-values for the shallow crack specimen arises along with a more prominent role of the Weibull modulus, m, on the constraint correlation ($J^{a/W=0.2}_{SEB} \rightarrow J^{a/W=0.5}_{SEB}$). Observe that the J-values for the shallow crack specimen, $J^{a/W=0.2}_{SEB}$, can be as high as $3 \sim 4$ times the corresponding J-values for the deep crack configuration, $J^{a/W=0.5}_{SEB}$. Further, note that the toughness ratios are also relatively insensitive to the adopted function Ψ_c when plastic strain effects are included into the analysis.

6. Concluding remarks

We have presented an extensive survey coupled with further developments of a probabilistic framework for cleavage fracture which incorporates weakest link statistics and a micromechanics model reflecting the critical instability of Griffith-like microcracks across microstructural boundaries. The approach addresses the strong effects of constraint variations on (macroscopic) cleavage fracture toughness which also includes the influence of plastic strain on the number of eligible Griffith-like microcracks nucleated from brittle particles dispersed into the ferrite matrix. A modified Weibull stress ($\tilde{\sigma}_w$) incorporating plastic strain effects on cleavage fracture emerges as a probabilistic fracture parameter to define conditions leading to (local) material failure. Unstable crack propagation occurs at a critical value of $\tilde{\sigma}_w$ which provides support to develop a toughness scaling methodology to unify toughness measures across different crack configurations and loading modes. Approximate treatments of plastic strain effects are outlined serving to define simple functions of plastic strain, expressed in terms of Ψ_c, entering directly into the limiting distribution for fracture stress.

Our approach differs from previous extensions of a local approach to cleavage fracture incorporating plastic strain effects, including the works of Bordet et al. [58,59] and Margolin et al. [65,56], primarily in the choice of the model to describe the influence of plastic strain on cleavage microcracking. While we make no claim that our model provides a unique manner to adequately treat the coupling of constraint and plastic strain effects on fracture toughness predictions, the present

methodology is statistically consistent and provides tenable results consistent with experimental observations. Undoubtedly, both approaches share common features in the sense of altering the evolution of the Weibull stress (interpreted as a probabilistic crack driving force in the present context) with increased loading by a functional form of plastic strain.

The small-scale yielding analyses under varying levels of T-stress presented in our study provide valuable insight about the effects of plastic strain and the adopted form for Ψ_c on fracture resistance. These SSY results exhibit the essential features of the micromechanics approach in correlating macroscopic fracture toughness with the various descriptions of plastic strain effects. While the fracture resistance, here characterized in terms of the evolution of $\tilde{\sigma}_w$ with loading, depends on the adopted plastic strain model (since each adopted function Ψ_c defines different fractions of Griffith-like microcracks which are eligible to propagate unstably), the influence of key parameters related to Ψ_c are relatively small.

3-D analyses of deep and shallow crack SE(B) specimens with various flow and hardening properties illustrate the predictive capability of the present probabilistic formulation through recourse to a toughness scaling methodology based upon $\tilde{\sigma}_w$. The influences of hardening behavior and near-tip plastic strains (coupled with the evolving near-tip stresses) on fracture behavior are examined based on predictions of toughness ratios for crack-tip conditions corresponding to low constraint and large scale deformation. The present study clearly shows important features associated with the inclusion of plastic strain effects into the Weibull stress model which are not fully accounted in conventional analyses using the standard Beremin model. Indeed, while plastic strain effects on cleavage fracture are treated approximately, albeit highly compatible with experimental observations, our parameter results largely support the present approach, particularly in fracture assessments of moderate-to-low hardening materials.

An unexpected result emerging from our analyses is the relatively weak effect of the adopted plastic strain models and associated function Ψ_c on the constraint correlations of J-values in the SE(B) specimens. While conceptually different, the mathematical translation of such models into simple statistical distributions of plastic strain does not uncover the strong exponential character of the function Ψ_c, particularly in the case of the exponential dependence model and the particle fracture stress model. The function Ψ_c corresponding to the microcrack density model does not possess an exponential character describing the effects of plastic strain on cleavage fracture but it nevertheless resembles the latter models. Effectively, the number of eligible Griffith-like microcracks is controlled by an exponential form of plastic strain in both specimen geometries which may plausibly justify the general features exhibited by these toughness correlation results. Overall, inclusion of plastic strain effects into the probabilistic framework to describe cleavage fracture does reduce the amount of constraint correction from shallow-to-deep notch SE(B) fracture specimens, which is generally consistent with available toughness data.

However, because of the rather strong sensitivity of the calibrated Weibull modulus, m, on the adopted plastic strain model, it is somewhat difficult to draw definitive conclusions on the effectiveness of the present framework incorporating various forms of Ψ_c on fracture assessments and toughness predictions for low constraint crack configurations. While the analyses presented here favor comparisons of toughness correlations derived from the various plastic strain models based on fixed values of the Weibull modulus, the applicability of the modified Weibull stress model in fracture predictions using experimentally measured cleavage fracture toughness values (rather than chosen for convenient reasons) remains untested. This issue and related aspects will be taken up in Part II of this study which describes applications of the probabilistic framework and the modified Weibull stress to assess constraint effects in precracked Charpy (PCVN) specimens and to predict the reference temperature, T_0, for a pressure vessel steel. Nevertheless, the present study advances current understanding of probabilistic modeling for cleavage fracture while, at the same time, providing compelling support for developing fracture assessment methodologies based on $\tilde{\sigma}_w$.

Acknowledgments

This investigation is supported by Fundação de Amparo à Pesquisa do Estado de São Paulo (FAPESP) through Grant 2012/13053-2 and by the Brazilian Council for Scientific and Technological Development (CNPq) through Grants 473975/2012-2 and 306193/2013-2. The second author (RHD) was supported by the M.T. Geoffrey Yeh Fund at the University of Illinois at Urbana-Champaign.

References

[1] Hutchinson JW. Fundamentals of the phenomenological theory of nonlinear fracture mechanics. J Appl Mech 1983;50:1042–51.
[2] Anderson TL. Fracture mechanics: fundamentals and applications. 3rd ed. Boca Raton (FL): CRC Press; 2005.
[3] Dodds RH, Shih C, Anderson T. Continuum and micro-mechanics treatment of constraint in fracture. Int J Fract 1993;64:101–33.
[4] Al-Ani AM, Hancock JW. J-dominance of short cracks in tension and bending. J Mech Phys Solids 1991;39:23–43.
[5] Betegon C, Hancock JW. Two-parameter characterization of elastic-plastic crack tip fields. J Appl Mech 1991;58:104–13.
[6] Parks DM. Advances in characterization of elastic-plastic crack-tip fields. In: Argon AS, editor. Topics in fracture and fatigue. Springer Verlag; 1992. p. 59–98.
[7] O'Dowd N, Shih C. Family of crack-tip fields characterized by a triaxiality parameter: Part I – structure of fields. J Mech Phys Solids 1991;39:989–1015.
[8] O'Dowd N, Shih C. Family of crack-tip fields characterized by a triaxiality parameter: Part II – fracture applications. J Mech Phys Solids 1992;40:939–63.
[9] Yang S, Chao YJ, Sutton MA. High order asymptotic crack tip fields in a power-law hardening material. Engng Fract Mech 1993;45:1–20.
[10] Chao XK, Chao YJ. J-$A2$ characterization of crack-tip fields: extent of J-$A2$ dominance and size requirements. Int J Fract 1998;89:285–307.
[11] Beremin FM. A local criterion for cleavage fracture of a nuclear pressure vessel steel. Metall Mater Trans A 1983;14:2277–87.
[12] Mudry F. A local approach to cleavage fracture. Nucl Engng Des 1987;105:65–76.
[13] Pineau A. Development of the local approach to fracture over the past 25 years: theory and applications. Int J Fract 2006;138:139–66.
[14] Mann NR, Schafer RE, Singpurwalla ND. Methods for statistical analysis of reliability and life data. New York: Jonh Wiley & Sons; 1974.

[15] McMahon CJ, Cohen M. Initiation of cleavage in polycrystalline iron. Acta Metall 1965;13:591–604.
[16] Kaechele LE, Tetelman AS. A statistical investigation of microcrack formation. Acta Metall 1969;17:463–75.
[17] Brindley BJ. The effect of dynamic strain-aging on the ductile fracture process in mild steel. Acta Metall 1970;18:325–9.
[18] Lindley TC, Oates G, Richards CE. A critical appraisal of carbide cracking mechanism in ferritic/carbide aggregates. Acta Metall 1970;18:1127–36.
[19] Gurland J. Observations on the fracture of cementite particles in a spheroidized 1.05% C steel deformed at room temperature. Acta Metall 1972;20:735–41.
[20] Ruggieri C. Influence of threshold parameters on cleavage fracture predictions using the Weibull stress model. Int J Fract 2001;110:281–304.
[21] Ruggieri C. An engineering methodology to assess effects of weld strength mismatch on cleavage fracture toughness using the Weibull stress approach. Int J Fract 2010;164:231–52.
[22] Averbach BL. Micro and macro formation. Int J Fract Mech 1965;1:272–90.
[23] Tetelman AS, McEvily AJ. Fracture of structural materials. New York: John Wiley & Sons; 1967.
[24] Smith E. Cleavage fracture in mild steel. Int J Fract Mech 1968;4:131–45.
[25] Low JR. Relation of properties to microstructure. Trans Am Soc Met 1953;46A:163–79.
[26] Owen WS, Averbach M, Cohen BL. Brittle fracture in mild steel in tension at −196 °C. Trans Am Soc Met 1958;50:634–55.
[27] Griffith AA. The phenomenon of rupture and flow in solids. Philos Trans Roy Soc, Ser A 1921;221:163–98.
[28] Curry DA, Knott JF. Effects of microstructure on cleavage fracture stress in steel. Met Sci 1978;12:511–4.
[29] Curry DA, Knott JF. Effects of microstructure on cleavage fracture toughness of quenched and tempered steels. Met Sci 1979;13:341–54.
[30] Hahn GT. The influence of microstructure on brittle fracture toughness. Metall Trans A 1984;15:947–59.
[31] Xia L, Shih CF. Ductile crack growth – III: transition to cleavage fracture incorporating statistics. J Mech Phys Solids 1996;44:603–39.
[32] Wallin K, Laukkanen A. New developments of the Wallin, Saario, Törrönen cleavage fracture model. Engng Fract Mech 2008;75:3367–77.
[33] Fairchild DP, Howden DG, Clark WAT. The mechanism of brittle fracture in a microalloyed steel: Part II – mechanistic modeling. Metall Mater Trans A 2000;31A:653–67.
[34] Weibull W. The phenomenon of rupture in solids. Handlingar 153. Ingeniors Vetenskaps Akademien; 1939.
[35] Weibull W. A statistical theory of the strength of materials. Handlingar 151. Ingeniors Vetenskaps Akademien; 1939.
[36] Epstein B. Statistical aspects of fracture problems. J Appl Phys 1948;19:140–7.
[37] Freudenthal AM. Statistical approach to brittle fracture. In: Liebowitz H, editor. Fracture: an advanced treatise, vol. II. New York: Academic Press; 1968. p. 592–619 [chapter 6].
[38] Fisher RA, Tippet LHC. Limiting forms of the frequency distribution of the largest and smallest member of a sample. Proc Cambridge Philos Soc 1928;24:180–90.
[39] Gumbel EJ. Statistics of extremes. New York: Columbia University Press; 1958.
[40] Kendall MG, Stuart A. The advanced theory of statistics. 2nd ed. New York: Hafner; 1967.
[41] Evans AG, Langdon TG. Structural ceramics. In: Chalmers B, editor. Progress in materials science, vol. 21. New York: Pergamon Press; 1976. p. 171–441.
[42] McClintock FA, Argon AS. Mechanical behavior of materials. Reading (MA): Addison-Wesley; 1966.
[43] Batdorf SB, Crose JG. A statistical theory for the fracture of brittle structures subjected to nonuniform polyaxial stresses. J Appl Mech 1974;41:459–64.
[44] Evans AG. A general approach for the statistical analysis of multiaxial fracture. J Am Ceram Soc 1978;61:302–8.
[45] McClintock FA, Zaverl JR. An analysis of the mechanism and statistics of brittle crack initiation. Int J Fract 1979;15:107–18.
[46] Matsuo Y. Statistical theory for multiaxial stress states using Weibull's three-parameter function. Engng Fract Mech 1981;14:527–38.
[47] Lin T, Evans AG, Ritchie RO. A statistical model of brittle fracture by transgranular cleavage. J Mech Phys Solids 1986;21:263–77.
[48] Godse R, Gurland J. A statistical model for low temperature cleavage fracture in mild steels. Acta Metall 1989;37:541–8.
[49] Wallin K, Saario T, Törrönen K. Statistical model for carbide induced brittle fracture in steel. Met Sci 1984;18:13–6.
[50] Pineau A. Global and local approaches of fracture – transferability of laboratory test results to components. In: Argon AS, editor. Topics in fracture and fatigue. Springer Verlag; 1992. p. 197–234.
[51] Minami F, Brückner-Foit A, Munz B, Trolldenier D. Estimation procedure for the Weibull parameters used in the local approach. Int J Fract 1992;54:197–210.
[52] Ruggieri C, Dodds RH. A transferability model for brittle fracture including constraint and ductile tearing effects: a probabilistic approach. Int J Fract 1996;79:309–40.
[53] Gao X, Ruggieri C, Dodds R. Calibration of Weibull stress parameters using fracture toughness data. Int J Fract 1998;92:175–200.
[54] Petti JR, Dodds RH. Calibration of the Weibull stress scale parameter, σ_u, using the master curve. Engng Fract Mech 2005;72:91–120.
[55] Margolin BZ, Shvetsova VA. Local criterion to for cleavage fracture: structural and mechanical approach. J Phys IV 1996;6:225–34.
[56] Margolin BZ, Shvetsova VA, Gulenko AG, Kostylev VI. Prometey local approach to brittle fracture: development and application. Engng Fract Mech 2008;75:3483–98.
[57] Margolin BZ, Shvetsova VA, Gulenko AG. Radiation embrittlement modeling in multi-scale approach to brittle fracture of RPV steels. Int J Fract 2012;179:87–108.
[58] Bordet SR, Karstensen AD, Knowles DM, Wiesner CS. A new statistical local criterion for cleavage fracture in steel. Part I: model presentation. Engng Fract Mech 2005;72:435–52.
[59] Bordet SR, Karstensen AD, Knowles DM, Wiesner CS. A new statistical local criterion for cleavage fracture in steel. Part II: application to an offshore structural steel. Engng Fract Mech 2005;72:453–74.
[60] Gao X, Zhang G, Srivatsan TS. Prediction of cleavage fracture in ferritic steels: a modified Weibull stress model. Mater Sci Engng A 2005;394:210–9.
[61] Feller W. Introduction to probability theory and its application, vol. I. New York: John Wiley & Sons; 1957.
[62] Gao X, Dodds RH. Constraint effects on the ductile-to-brittle transition temperature of ferritic steels: a Weibull stress model. Int J Fract 2000;102:43–69.
[63] American Society for Testing and Materials. Standard test method for determination of reference temperature, T_0, for ferritic steels in the transition range. ASTM E1921-13a; 2013.
[64] Wallin K, Saario T, Törrönen K. Fracture of brittle particles in a ductile matrix. Int J Fract 1987;32:201–9.
[65] Margolin BZ, Gulenko AG, Shvetsova VA. Improved probabilistic model for fracture toughness prediction for nuclear pressure vessel steels. Int J Press Ves Pip 1998;75:843–55.
[66] Wallin K, Laukkanen A. Aspects of cleavage fracture initiation – relative influence of stress and strain. Fatigue Fract Engng Mater Struct 2006;29:788–98.
[67] Kroon M, Faleskog J. A probabilistic model for cleavage fracture with a length scale influence of material parameters and constraint. Int J Fract 2002;118:99–118.
[68] Rice JR. Mechanics of crack tip deformation and extension by fatigue. In: Grosskreutz J, editor. Fatigue crack propagation. ASTM STP 415. Philadelphia: American Society for Testing and Materials; 1967. p. 247–311.
[69] Williams ML. On the stress distribution at the base of a stationary crack. J Appl Mech 1957;24:109–14.
[70] Nevalainen M, Dodds RH. Numerical investigation of 3-D constraint effects on brittle fracture in SE(B) and C(T) specimens. Int J Fract 1995;74:131–61.
[71] McMeeking RM. Finite deformation analysis of crack-tip opening in elastic-plastic materials and implications for fracture. J Mech Phys Solids 1977;25:357–81.
[72] Healy B, Gullerud A, Koppenhoefer K, Roy A, RoyChowdhury S, Petti J, et al. WARP3D: 3-D nonlinear finite element analysis of solids for fracture and fatigue processes. Tech rep. University of Illinois at Urbana-Champaign; 2014. <http://code.google.com/p/warp3d>.
[73] Moran B, Shih CF. A general treatment of crack tip contour integrals. Int J Fract 1987;35:295–310.

[74] Ruggieri C. FRACTUS2D: numerical computation of fracture mechanics parameters for 2-D cracked solids. Tech rep. University of Sao Paulo; 2011.
[75] Ruggieri C, Dodds RH. A Weibull stress approach incorporating the coupling effect of constraint and plastic strain in cleavage fracture toughness predictions. In: ASME 2014 pressure vessels & piping conference (PVP 2014), Anaheim, CA; 2014.
[76] Gao X, Dodds RH, Tregoning RL, Joyce JA, Link LR. A Weibull stress model to predict cleavage fracture in plates containing surface cracks. Fatigue Fract Engng Mater Struct 1999;22:481–93.
[77] Silva LAL, Cravero S, Ruggieri C. Correlation of fracture behavior in high pressure pipelines with axial flaws using constraint designed test specimens – Part II: 3-D effects on constraint. Engng Fract Mech 2006;76:2123–38.
[78] Dodds R, Anderson T, Kirk M. A framework to correlate a/W ratio effects on elastic-plastic fracture toughness (J_c). Int J Fract 1991;48:1–22.
[79] Anderson T, Dodds R. Specimen size requirements for fracture toughness testing in the ductile-brittle transition region. J Test Eval 1991;19:123–34.